Fog2 is critical for cardiac function and maintenance of coronary vasculature in the adult mouse heart

Bin Zhou,[1,2] Qing Ma,[1] Sek Won Kong,[1] Yongwu Hu,[1,3] Patrick H. Campbell,[4] Francis X. McGowan,[4] Kate G. Ackerman,[5] Bingruo Wu,[6] Bin Zhou,[6] Sergei G. Tevosian,[7] and William T. Pu[1,2]

[1]Department of Cardiology, Children's Hospital Boston and Department of Genetics, Harvard Medical School, Boston, Massachusetts, USA. [2]Harvard Stem Cell Institute, Harvard University, Cambridge, Massachusetts, USA. [3]Department of Biology, Life Science School, Wenzhou Medical College, Wenzhou, Zhejiang, People's Republic of China. [4]Department of Anesthesiology, Perioperative and Pain Medicine, Children's Hospital Boston, Boston, Massachusetts, USA. [5]Department of Pediatrics and Department of Biomedical Genetics, University of Rochester Medical Center, Rochester, New York, USA. [6]Department of Genetics, Albert Einstein College of Medicine, New York, New York, USA. [7]Department of Genetics and Norris Cotton Cancer Center, Dartmouth Medical School, Hanover, New Hampshire, USA.

Aberrant transcriptional regulation contributes to the pathogenesis of both congenital and adult forms of heart disease. While the transcriptional regulator friend of Gata 2 (FOG2) is known to be essential for heart morphogenesis and coronary development, its tissue-specific function has not been previously investigated. Additionally, little is known about the role of FOG2 in the adult heart. Here we used spatiotemporally regulated inactivation of *Fog2* to delineate its function in both the embryonic and adult mouse heart. Early cardiomyocyte-restricted loss of *Fog2* recapitulated the cardiac and coronary defects of the *Fog2* germline murine knockouts. Later cardiomyocyte-restricted loss of *Fog2* (*Fog2*^{MC}) did not result in defects in cardiac structure or coronary vessel formation. However, *Fog2*^{MC} adult mice had severely depressed ventricular function and died at 8–14 weeks. *Fog2*^{MC} adult hearts displayed a paucity of coronary vessels, associated with myocardial hypoxia, increased cardiomyocyte apoptosis, and cardiac fibrosis. Induced inactivation of *Fog2* in the adult mouse heart resulted in similar phenotypes, as did ablation of the FOG2 interaction with the transcription factor GATA4. Loss of the FOG2 or FOG2-GATA4 interaction altered the expression of a panel of angiogenesis-related genes. Collectively, our data indicate that FOG2 regulates adult heart function and coronary angiogenesis.

Introduction

Heart disease is a leading cause of morbidity and mortality in both infancy and adulthood. Congenital and adult heart disease have both been linked to altered regulation of cardiac gene transcription (1). Intriguingly, the same core set of transcriptional regulators governs cardiac transcription in both the developing and adult heart. Study of these cardiac transcription factors and their interaction is therefore critical in order to better understand the pathogenesis of cardiac malformation and cardiac failure.

The zinc finger transcription factor GATA4 is essential in both heart development and maintenance of postnatal heart function. GATA4 is expressed in cardiomyocytes and their mesodermal precursors and also in the endocardium and the epicardium (2, 3). Embryos lacking functional GATA4 arrested in development due to a defect in the visceral endoderm that caused aberrant ventral morphogenesis and cardiac bifida (4, 5). Using a conditional, tissue-restricted gene inactivation approach, we previously showed that normal cardiac morphogenesis requires myocardial expression of GATA4 (6) and that the development of heart valves also requires GATA4 expression in endocardial-derived cells (2). In the adult heart, GATA4 is a critical regulator of cardiac gene expression, cardiomyocyte differentiation and survival, and the adaptive response of adult hearts to biomechanical stress (7, 8). In addition, GATA4 was recently identified as a key regulator of cardiac angiogenesis in the adult heart (9).

The zinc finger transcriptional regulator FOG2 (friend of Gata 2, also known as ZFPM2) likewise plays an essential role in heart morphogenesis and development of coronary vessels (10, 11). *Fog2*$^{-/-}$ embryos died around E13.5 with cardiac defects, including thin myocardium, large ventricular septal defect (VSD), severe atrioventricular (AV) endocardial cushion defect, overriding aorta, and severe underdevelopment of the coronary vascular plexus. Transgenic mice expressing *Fog2* under the control of the cardiomyocyte-restricted *Myh6* (myosin, heavy polypeptide 6, cardiac muscle, α, also known as α-MHC) promoter partly rescued coronary development, but other cardiac morphological abnormalities persisted (11). This indicates that *Fog2* is required at a time or in a tissue compartment that is not impacted by the *Myh6-Fog2* transgene. FOG2 lacks intrinsic DNA binding ability. Rather, FOG2 influences gene transcription by specifically interacting with other transcription factors, most notably GATA4 (12). Missense mutation of *Gata4* (encoding GATA4[V217G]) disrupted GATA4-FOG2 interaction, without altering protein expression or DNA binding (13). Mice homozygous for this mutant allele (named *Gata4*^{ki}) develop severe heart defects similar to those seen in *Fog2*-null embryos, including aberrant coronary vessel development (13).

Fog2$^{-/-}$ and *Gata4*$^{ki/ki}$ embryos died around E13.5, precluding investigation of *Fog2* function in later stages of heart development

Conflict of interest: The authors have declared that no conflict of interest exists.

Nonstandard abbreviations used: AV, atrioventricular; Dox, doxycycline; EMT, epithelial-to-mesenchymal transition; EPDC, epicardium-derived cell; FOG2, friend of Gata 2; MIBI, ^{99m}Tc-2-methoxy isobutyl isonitrile; qRT-PCR, quantitative RT-PCR; VSD, ventricular septal defect.

Citation for this article: *J. Clin. Invest.* **119**:1462–1476 (2009). doi:10.1172/JCI38723.

and in the adult heart. Here we used a spatiotemporally regulated gene inactivation approach to delineate the role of *Fog2* both in embryo and adult heart. We found that early myocardial expression of *Fog2* is required for cardiac morphogenesis and coronary vascular development. Later myocardial inactivation of *Fog2* was compatible with normal heart development but resulted in heart failure associated with underdevelopment of coronary vessels. This was recapitulated by induced cardiomyocyte-restricted *Fog2* inactivation in the adult heart, demonstrating a continuing requirement for *Fog2* in maintenance of heart function and coronary vasculature. Mice that expressed only the mutant GATA4[V217G] protein in the myocardium also developed heart failure and dropout of coronary vasculature. Collectively, our results demonstrate that cardiomyocyte expression of *Fog2* is required for maintenance of myocardial and coronary vessel function in the adult heart.

Results

Early and late inactivation of Fog2 in fetal myocardium. To analyze the expression of *Fog2* during heart development, we studied $Fog2^{Lz/+}$ embryos, in which the *LacZ* reporter gene was driven by *Fog2* regulatory elements. X-gal staining showed that *Fog2* was robustly expressed in the heart and proepicardium from E9.5 to E11.5 (Figure 1A). In sections, we detected *Fog2* expression in atrial and ventricular myocardium, epicardium, endocardium, and endocardial cushions (Figure 1B). As *Fog2* was expressed in these different lineages, and previous work showed that transgenic *Fog2* expression in cardiomyocytes only partially rescued the cardiac defects of $Fog2^{-/-}$ embryos (11), we sought to further define the tissue-restricted requirement of *Fog2* for normal heart morphogenesis.

In order to study the temporal and spatial requirements for *Fog2* in heart development, we took a conditional loss-of-function approach, using a floxed *Fog2* allele ($Fog2^{fl}$) (14). Recombination of $Fog2^{fl}$ by Cre recombinase deleted exon 8, yielding a nonfunctional allele that did not express FOG2 protein (14). We achieved early cardiomyocyte-restricted deletion of *Fog2* using Cre recombinase expressed from NK2 transcription factor related, locus 5 regulatory elements ($Nkx2\text{-}5^{Cre}$). (15). $Nkx2\text{-}5^{Cre}$ catalyzed efficient recombination of floxed targets in cardiomyocytes by E9.5 (6, 15). While FOG2 was readily detectable in cardiomyocytes of $Fog2^{fl/-}$ $Nkx2\text{-}5^{+/+}$ control embryos (Figure 1C), FOG2 was not detectable in cardiomyocytes by E9.5 in $Fog2^{fl/-}Nkx2\text{-}5^{Cre/+}$ ($Fog2^{NK}$) embryos (Figure 1D). FOG2 was not significantly recombined in endocardium or AV cushion mesenchymal cells of $Fog2^{NK}$ embryos, consistent with cardiomyocyte-restricted recombination of $Fog2^{fl}$ by $Nkx2\text{-}5^{Cre}$ (Figure 1D). Cardiomyocyte recombination by $Nkx2\text{-}5^{Cre}$ was confirmed using the $Rosa26^{fsLz/+}$ reporter, which expresses β-gal only after Cre-mediated recombination. In $Fog2^{NK}$ embryos that also carried this reporter, β-gal was expressed in cardiomyocytes by E9.5 (Figure 1D). Cardiomyocyte *Fog2* inactivation in $Fog2^{NK}$ hearts was also confirmed by immunohistochemistry at E12.5 (Supplemental Figure 1; supplemental material available online with this article; doi:10.1172/JCI38723DS1).

In order to inactivate *Fog2* at a later developmental stage, we used the *Myh6-Cre* transgene, in which Cre recombinase is driven by the cardiomyocyte-specific α-MHC promoter. Robust recombination in *Myh6-Cre* embryos occurred at E11.5 to E12.5 (6, 16). FOG2 immunostaining at E9.5 and E12.5 delineated the spatiotemporal pattern of $Fog2^{fl}$ recombination by *Myh6-Cre* (Figure 1, E–H). FOG2 expression was not significantly different between $Fog2^{fl/-}$*Myh6-Cre* ($Fog2^{MC}$) and littermate Cre-nontransgenic control ($Fog2^{fl/-}NTg$) embryos at E9.5 (Figure 1, E and F). However, at E12.5, $Fog2^{MC}$ embryos displayed cardiomyocyte-restricted loss of FOG2 (Figure 1H). The later activity of *Myh6-Cre* was confirmed using the $Rosa26^{fsLz/+}$ reporter in $Fog2^{MC}$ embryos. At E9.5, β-gal expression was not detectable in the $Fog2^{MC}$ heart (Figure 1F), while at E12.5, *Fog2* was inactivated and β-gal was robustly expressed in most cardiomyocytes (Figure 1H).

Early cardiomyocyte-restricted ablation of *Fog2* in $Fog2^{NK}$ embryos resulted in lethality by E13.5–E14.5. $Fog2^{NK}$ embryos developed subcutaneous edema, hemorrhage, and pericardial effusion, suggesting severe impairment of cardiac function (Figure 2, A and B). $Fog2^{NK}$ hearts had a constellation of defects that largely recapitulated the abnormalities seen in *Fog2*-null hearts (10, 11), including large atrial septal defect and VSD, AV endocardial cushion defect, thin compact myocardium, and overriding aorta (Figure 2, C–H). The coronary vascular plexus of $Fog2^{NK}$ mutants was dramatically decreased compared with that of littermates with any of the 3 control genotypes (Figure 2, I–K, and Supplemental Figure 2). To further corroborate the above findings, we visualized the coronary plexus of $Fog2^{NK}$ mutant and control embryos in which a *LacZ* reporter gene was driven by the endothelial-restricted *Tie2* promoter (*Tie2-Lz*) transgene, which drives β-gal expression in endothelial cells (Figure 2, L and M). Control embryos demonstrated normal growth of the compact myocardium and multiple intramyocardial coronary vessels (Figure 2L). In contrast, $Fog2^{NK}$ hearts had very thin compact myocardium that contained few coronary vessels (Figure 2M).

To study the function of myocardial *Fog2* at later time points, we examined cardiac anatomy and coronary vascular development of $Fog2^{MC}$ embryos at E14.5. H&E staining of heart sections did not show structural heart defects in $Fog2^{MC}$ embryos (Supplemental Figure 3, A and B). The coronary vascular plexus formed normally, as demonstrated by whole-mount staining for the endothelial marker PECAM (Supplemental Figure 3, C and D). Sections of whole-mount stained hearts showed that the compact myocardium thickened normally and contained a normal number of intramyocardial coronary vessels (Supplemental Figure 3, E and F). Consistent with normal cardiac morphogenesis and coronary vascular development, $Fog2^{MC}$ mice survived to weaning at the expected Mendelian frequency (Table 1).

Fog2 deletion in epicardium, endocardium, and neural crest-derived cells. In addition to cardiomyocytes, several additional lineages are required for cardiac morphogenesis, including the epicardium, endocardium, and cardiac neural crest (17, 18). To determine whether *Fog2* is required in these lineages, we used a panel of Cre alleles to inactivate *Fog2* in each (Table 1).

To inactivate *Fog2* in the epicardium, we used Cre knocked into the Wilms tumor 1 (*Wt1*) locus ($Wt1^{GFPCre/+}$) (19). WT1 and Cre expression was restricted to the epicardium (Supplemental Figure 4, A and B). Epicardium-derived cells (EPDCs), labeled using $Wt1^{GFPCre}$, were found within the myocardium (Supplemental Figure 4C). These EPDCs have been implicated in coronary vessel development (20). However, epicardial deletion of *Fog2* by $Wt1^{GFPCre/+}$ did not impair coronary vascular development (Supplemental Figure 4D), suggesting that *Fog2* is dispensable in epicardium and EPDCs for this process. However, $Fog2^{fl/-}Wt1^{GFPCre/+}$ fetuses developed severe AV endocardial cushion defects and thin myocardium at later developmental stages (Supplemental Figure 4E), and pups died in the perinatal period (Table 1 and data not shown). These data indicated that *Fog2* expression in epicardium or its derivatives is required for normal growth and development of the AV valves and the compact myocardium.

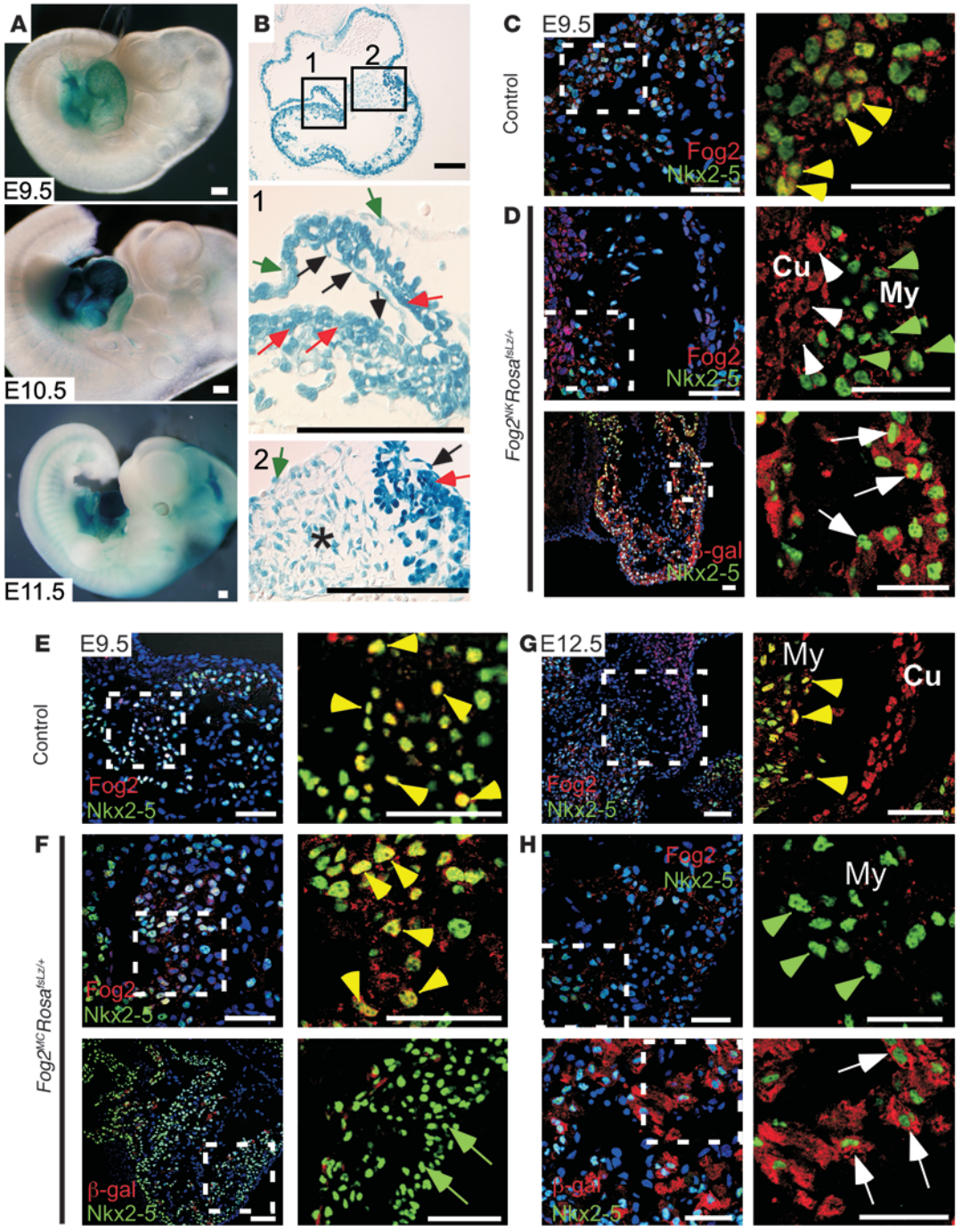

Figure 1

Temporal tissue-restricted inactivation of *Fog2*. (**A**) Whole-mount X-gal staining of E9.5–E11.5 $Fog2^{Lz/+}$ embryos. (**B**) Section of an E10.5 $Fog2^{Lz/+}$ embryo stained with X-gal. *Fog2* was expressed in cardiomyocytes (1, red arrows), epicardial cells (black arrows), endocardial cells (green arrows), and AV cushion mesenchymal cells (2, asterisk). (**C** and **D**) Immunohistochemical staining for FOG2 (red) and NKX2-5 (green; cardiomyocyte marker). At E9.5, FOG2 was readily detected in $Fog2^{fl/-}$ control cardiomyocytes (yellow arrowheads). In littermate $Fog2^{NK}$ heart, FOG2 immunoreactivity was lost in myocardium (My, green arrowheads) but remained in endocardial cushion (Cu, white arrowheads). Staining of $Fog2^{NK}Rosa26fs^{Lz/+}$ for Cre-activated β-gal expression (red) confirmed recombination in cardiomyocytes at E9.5 (green; white arrows). (**E** and **F**) In $Fog2^{MC}Rosa^{fsLz/+}$ and $Fog2^{fl/-}$ hearts, at E9.5 FOG2 (red) was expressed in cardiomyocytes (green NKX2-5 staining; yellow arrowheads). At this stage, the *Myh6-Cre* transgene has not yet catalyzed efficient recombination, as indicated by lack of robust β-gal expression from the Cre-activated reporter (green arrows). (**G** and **H**) At E12.5, FOG2 immunoreactivity was readily detected in $Fog2^{fl/-}$ control cardiomyocytes (yellow arrowheads) but not $Fog2^{MC}$ mutant cardiomyocytes (green arrowheads). The Cre-activated reporter robustly expressed β-gal in cardiomyocytes at E12.5 (white arrows). Scale bar: 50 μm. All box regions indicate the magnified figures on right sides (**C**–**H**).

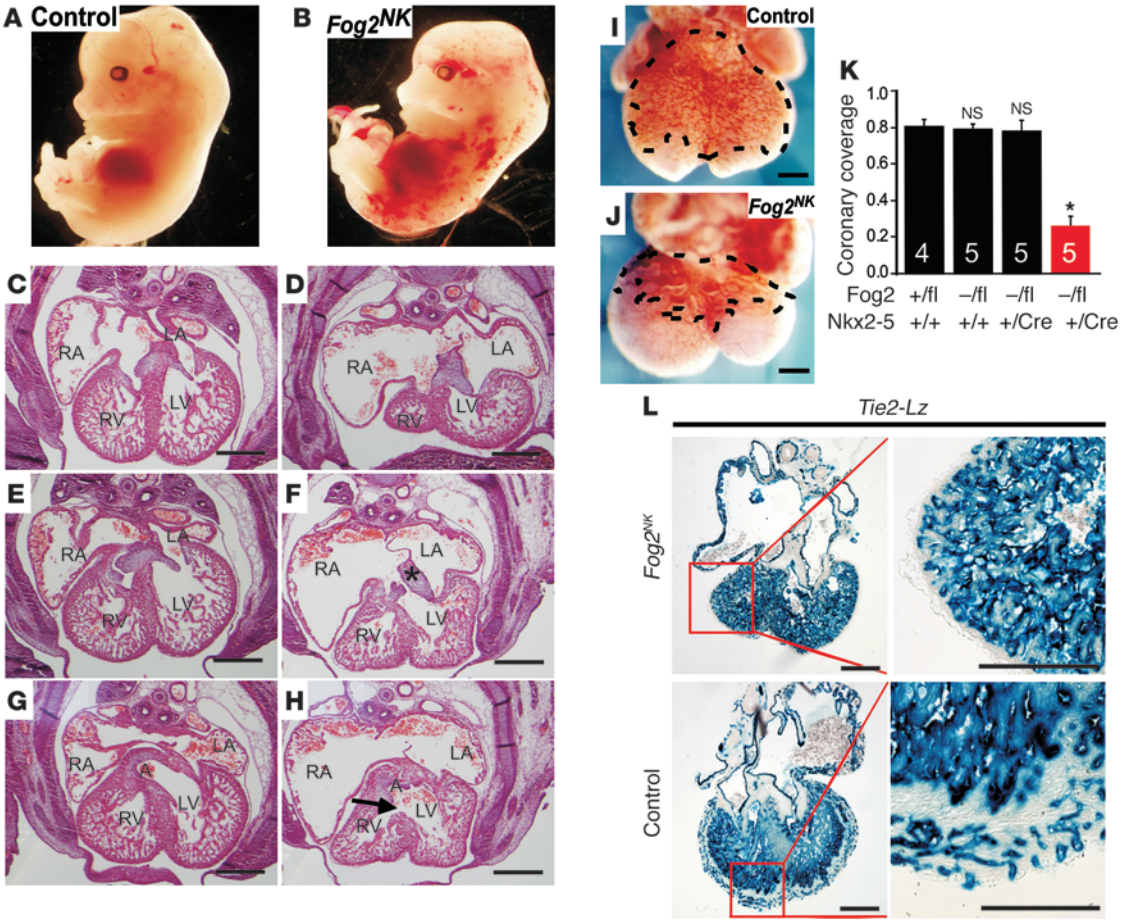

Figure 2
Abnormal heart development and coronary vasculogenesis after early cardiomyocyte-restricted *Fog2* inactivation. (**A** and **B**) Control (*Fog2*$^{fl/+}$*Nkx2-5*$^{Cre/+}$) and littermate *Fog2*^{NK} mutant embryos at E13.5. (**C**–**H**) Representative H&E staining of *Fog2*^{NK} (right panels) and littermate control (left panels; *Fog2*$^{fl/+}$*Nkx2-5*$^{Cre/+}$) hearts at different levels. RA, right atrium; LA, left atrium; RV, right ventricle; A, aorta. The asterisk indicates AV cushion and the arrow indicates VSD. (**I**–**K**) PECAM whole-mount staining of *Fog2*^{NK} and control (*Fog2*$^{fl/+}$*Nkx2-5*$^{Cre/+}$) hearts at E13.5. The coronary endothelial plexus coverage (ratio of region within black dotted line to total projected ventricular area) was significantly decreased in mutants. (*$P < 0.05$; $n = 4$–5 per group as indicated.) (**L**) Section of X-gal stained *Tie2-Lz* hearts showed decreased coronary vessels in the compact myocardial layer of *Fog2*^{NK} mutant compared with *Fog2*$^{fl/+}$*Nkx2-5*$^{Cre/+}$ littermate control. Scale bar: 500 μm. Ventricles in the boxed regions are magnified (right panels).

To inactivate *Fog2* in the endocardium, we used a *Tie2Cre* transgene to drive endothelial-restricted recombination. *Tie2Cre* inactivation of *Fog2* (*Fog2*^{T2}) did not detectably impact coronary plexus, endocardial cushions, or compact myocardium development (Supplemental Figure 5, A and B), and the survival rate to weaning was normal (Table 1). Adult *Fog2*^{T2} mice had normal tricuspid and mitral valves (Supplemental Figure 5C). Functional redundancy with *Fog1* in endothelial-derived cells may contribute to the lack of phenotype in *Fog2*^{T2} mice (21).

To investigate the functional requirement of *Fog2* in cardiac neural crest, we used the *Wnt1-Cre* transgene (22), in which wingless-related MMTV integration site 1 (*Wnt1*) regulatory elements drive Cre expression in cardiac neural crest. *Fog2*$^{fl/-}$*Wnt1-Cre* mice survived normally to weaning and had no detectable defect in either heart morphogenesis or coronary development (Table 1 and data not shown).

Epicardial epithelial-to-mesenchymal transition is normal in Fog2$^{-/-}$ *heart*. Through an epithelial-to-mesenchymal transition (EMT), epicardial cells generate mesenchymal cells, which migrate into the subjacent myocardium (Supplemental Figure 4C) (19, 23, 24). Because epicardium and epicardial EMT are necessary for coronary vasculogenesis (20, 23), it was hypothesized that the coronary vascular defect of *Fog2*-null mutants was due to aborted epicardial EMT (11). To test this hypothesis, we first assessed the competence of *Fog2*-null epicardium to undergo EMT. When E12.5 *Fog2*$^{+/+}$ embryo heart apexes were cultured on a collagen gel, epicardium grew off the explant as an epithelial sheet. At the edge of this cobblestone-like epithelial sheet, a subset of cells delaminated from the sheet, adopted a spindle-like shape, migrated into the collagen gel, and expressed the mesenchymal marker SMA (Figure 3, A–C). The behavior of *Fog2*$^{-/-}$ explants was not significantly distinguishable from *Fog2*$^{+/+}$ explants in this assay (Figure 3D), indicating that *Fog2*$^{-/-}$ epicardial cells remain competent to undergo EMT.

Next, we asked if epicardial EMT occurs normally in *Fog2*$^{-/-}$ embryos. Epicardium was intact in *Fog2*$^{-/-}$ embryos, as demonstrated by staining for epicardium-specific markers WT1 and RALDH2 (Supplemental Figure 6). Therefore, we used Cre-loxP lineage trac-

Table 1
Tissue-restricted *Fog2* knockout

Tissue compartment	Cre line	No. at weaning	Expected Mendelian survival rate (%)	Phenotype
Endocardium	*Tie2Cre*	24	166%	No phenotype
Myocardium	*Nkx2-5^{Cre}*	129	0%[A]	Thin myocardium, ASD, VSD, decreased coronary vasculature, CAVC
	Myh6-Cre	55	110%	Embryo, normal; adult, heart failure
	TNT-iCre	92	115%	Embryo, normal, adult, normal; after induction, heart failure
Epicardium	*Wt1^{GFPCre}*	36	0%[A]	Death at P0, CDH, thin myocardium, CAVC, normal coronaries
Neural crest	*Wnt1-Cre*	35	114%	Normal survival

[A]*P*, significant by χ^2 analysis. ASD, atrial septal defect; CAVC, common atrioventricular canal; CDH, congenital diaphragmatic hernia.

ing to follow the fate of epicardial cells in *Fog2$^{+/+}$* compared with *Fog2$^{-/-}$* hearts (Supplemental Figure 4C). *Wt1^{GFPCre}* selectively activated *Rosa26^{fsLz}* in the epicardium and its derivatives (Figure 3E), labeling EPDCs with β-gal. In *Fog2$^{+/+}$Wt1$^{GFPCre/+}$Rosa26$^{fsLz/+}$* hearts, β-gal$^+$ EPDCs were observed within the myocardium (Figure 3F). In *Fog2$^{-/-}$ Wt1$^{GFPCre/+}$Rosa26$^{fsLz/+}$* hearts, there was no significant difference in the number of β-gal$^+$ EPDCs (Figure 3, F and G), indicating that epicardial EMT occurred normally in *Fog2* knockout embryos. Taken together, our data show that the coronary vasculogenesis defect in *Fog2* mutant embryos is not due to impaired epicardial EMT.

Fog2 is required for adult mouse survival and normal cardiac function. While *Fog2^{MC}* mice survived normally to weaning, they died at 8–12 weeks of age (Figure 4A) with signs and symptoms of heart failure, indicating that FOG2 is required for normal adult heart function. Efficient inactivation of *Fog2* was confirmed by quantitative RT-PCR (qRT-PCR) (Figure 4B). Echocardiography demonstrated that *Fog2^{MC}* hearts were dilated and had severely depressed fractional shortening, a measure of systolic contractile function (Figure 4C and Table 2). Ventricular dilatation and depressed contraction were also demonstrated by cardiac imaging via PET (Supplemental Videos 1 and 2). On histopathological examination, *Fog2^{MC}* hearts displayed cardiomegaly, wall thinning, and ventricular dilation (Figure 4, D and E). At an ultrastructural level, however, sarcomere and mitochondrial structure were preserved in *Fog2^{MC}* cardiomyocytes (Supplemental Figure 7, A and B), suggesting that the striking *Fog2^{MC}* phenotype is not attributable to gross sarcomere disorganization or mitochondrial abnormalities.

Consistent with the heart failure phenotype, natriuretic peptide precursor type A (*Anf*, also known as *Nppa*) and natriuretic peptide precursor type B (*Bnp*, also known as *Nppb*) mRNAs, molecular markers of heart failure, were upregulated in *Fog2^{MC}* hearts (Figure 4F). Although FOG2 was recently reported to regulate the sarcoplasmic reticulum Ca^{2+}-ATPase (*Serca2a*, also known as *ATP2a2*) (25), *Serca2* expression was not significantly changed in *Fog2^{MC}* hearts (Figure 4F) or in neonatal *Fog2$^{fl/fl}$* cardiomyocytes depleted of FOG2 by treatment with Cre adenovirus (data not shown). *Gata4* expression was also not significantly changed in *Fog2^{MC}* hearts (Figure 4F), indicating that heart failure in this model was not due to epistatic changes in *Gata4* expression.

Increased cardiomyocyte loss from apoptosis has frequently been observed in heart failure, and cardiomyocyte apoptosis can, by itself, cause cardiac failure (26, 27). To better understand the cellular mechanisms leading to heart failure in *Fog2^{MC}* mutants, we asked whether *Fog2* inactivation resulted in increased cardiomyocyte apoptosis. Cardiomyocyte apoptosis was significantly increased in *Fog2^{MC}* hearts compared with either *Fog2$^{fl/+}$Myh6-Cre* and *Fog2$^{fl/-}$NTg* controls, as determined by both TUNEL and activated caspase-3 staining (Figure 4, G–I). Consistent with increased cardiomyocyte apoptosis, fibrotic replacement of apoptotic myocardial tissues resulted in increased cardiac fibrosis in *Fog2^{MC}* hearts, as demonstrated by both trichrome and collagen III staining (Supplemental Figure 7, C–F).

Fog2 is required for normal myocardial perfusion and coronary angiogenesis. Based on defective coronary vasculogenesis observed in fetal *Fog2^{NK}* hearts, we hypothesized that abnormal coronary vasculature may contribute to the development of myocardial dysfunction and cardiomyocyte apoptosis in *Fog2^{MC}* hearts. In vivo injection of a latex polymer (Microfil) revealed decreased coronary vasculature in *Fog2^{MC}* hearts compared with control hearts (Figure 5, A–F). This was confirmed by tail vein injection of Bs-1 lectin, which stained endothelial cells that received effective blood flow (Figure 5G). Decreased myocardial perfusion was further confirmed by measuring myocardial uptake of ^{99m}Tc-2-methoxy isobutyl isonitrile (MIBI), which is proportional to myocardial perfusion. MIBI uptake was significantly decreased in *Fog2^{MC}* hearts (Figure 5H).

Decreased myocardial perfusion and increased cardiomyocyte apoptosis in *Fog2^{MC}* hearts suggested the possibility that the mutant myocardium was ischemic. To test this hypothesis, we injected the compound pimonidazole hydrochloride (hypoxyprobe), which forms protein adducts under hypoxic conditions. These protein adducts were visualized with specific antibodies. Hypoxyprobe immunoreactivity was substantially increased in *Fog2^{MC}* hearts compared with littermate *Fog2$^{fl/-}$NTg* controls (Figure 5, I and J). Both cardiomyocytes and interstitial cells were stained. These data indicated that diminished perfusion in *Fog2^{MC}* hearts resulted in tissue hypoxia, which likely contributed to elevated cardiomyocyte apoptosis.

Consistent with these findings, the density of PECAM$^+$ vessels, predominantly capillaries, was significantly diminished in *Fog2^{MC}* hearts compared with *Fog2$^{fl/+}$Myh6-Cre* and *Fog2$^{fl/-}$NTg* control hearts (204.1 ± 25.6 vs. 251.2 ± 13.0 and 255.0 ± 10.5 vessels/×40 field, respectively; $P < 0.05$; Figure 5K). The decreased density of endothelial cells was associated with increased endothelial cell apoptosis in *Fog2^{MC}* hearts, as demonstrated by quantitative analysis of TUNEL and activated caspase-3–stained sections (Figure 5M and Supplemental Figure 7J). SMA staining revealed that *Fog2^{MC}* hearts also had lower coronary arteriole density compared with *Fog2$^{fl/+}$Myh6-Cre* and *Fog2$^{fl/-}$NTg* control hearts (11.2 ± 3.5 vs. 21.1 ± 4.5 and 18.9 ± 3.8 vessels/×20 field, respectively; $P < 0.05$; Figure 5L). These results indicate that myocardial *Fog2* expression is essential for maintenance of coronary vasculature.

Induced inactivation of Fog2 in postnatal myocardium leads to cardiac failure. Fog2 is expressed in both fetal and adult heart (Figure 1 and

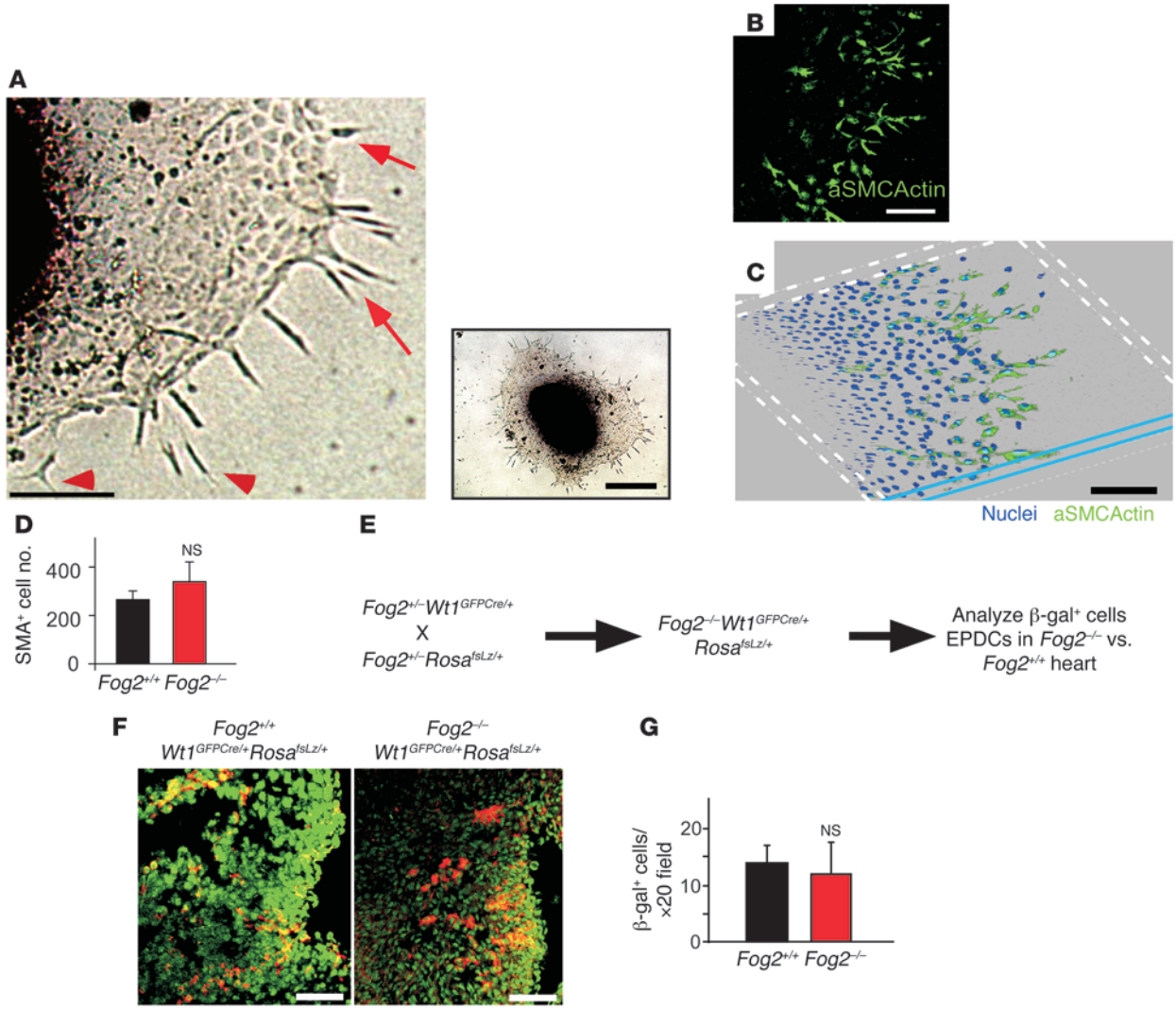

Figure 3

Normal EMT in *Fog2* mutant epicardium. (**A**) Representative figure of ex vivo heart explant on collagen gel. Cells transitioned to spindle-shaped mesenchymal cells (red arrows) at the edge of the epicardial outgrowth, and some delaminated from the epithelial sheet and migrated into collagen gel (red arrowheads). Inset shows an overview of the explant. (**B**) SMA staining (green) showed that most mesenchymal cells are at the edge of epicardial sheets. (**C**) A stack of confocal images of an explant cultured on a collagen gel, extending from the surface to the interior of the collagen gel, was acquired. Three-dimensional rendering showed migration of SMA+ cells into the gel. (**D**). Quantitation of the SMA cell number. EMT was not significantly different between $Fog2^{-/-}$ and $Fog2^{+/+}$ explants. $n = 4$. (**E**) Experimental outline of tracing the fate of EPDCs in *Fog2* mutants. Embryos were collected at E13.5. (**F**) Representative immunostaining for β-gal+ EPDCs in $Fog2^{-/-}$ and $Fog2^{+/+}$ hearts. (**G**) Lack of significant difference between number of β-gal+ EPDCs in mutant compared with control ($n = 3$). Scale bar: 50 μm.

Supplemental Figure 8, A–D). While the $Fog2^{MC}$ phenotype suggested that *Fog2* continues to have an important role in the adult heart, an alternate possibility was that the adult $Fog2^{MC}$ phenotype is an adult manifestation of a developmental phenotype. Therefore, to directly address the requirement of *Fog2* in the adult heart, we developed an inducible, cardiomyocyte-restricted *Fog2* inactivation model. We generated a Cre transgene, named *TNT-iCre*, by co-integrating 2 constructs, one containing the cardiac-specific troponin T promoter driving the reverse tet activator protein (rtTA) and the other containing a tet activator protein-dependent promoter driving Cre (Figure 6A). Administration of doxycycline (Dox) upregulates Cre expression in cardiomyocytes, resulting in Cre-mediated recombination of floxed targets. Dox-treated *TNT-iCre* strongly recombined the $Rosa26^{fsLz}$ reporter in cardiomyocytes (Supplemental Figure 8, E–G).

To inducibly inactivate *Fog2* in adult cardiomyocytes, we generated $Fog2^{fl/fl}$*TNT-iCre* mice (designated $Fog2^{iCre}$). Mice were treated with standard or Dox-containing drinking water from 4 to 8 weeks of age. Mice then underwent echocardiography and pathological examination. In the absence of Cre, Dox treatment of $Fog2^{fl/fl}$ mice did not significantly affect *Fog2* expression. In $Fog2^{iCre}$ hearts not treated with Dox ($Fog2^{iCre–Ctrl}$), *Fog2* expression was also not significantly changed, indicating minimal recombination in the absence of Dox. In contrast, *Fog2* expression in $Fog2^{iCre}$ hearts treated with Dox ($Fog2^{iCre–Dox}$) was significantly decreased, indicating efficient Dox-induced inactivation of *Fog2* (Figure 6B).

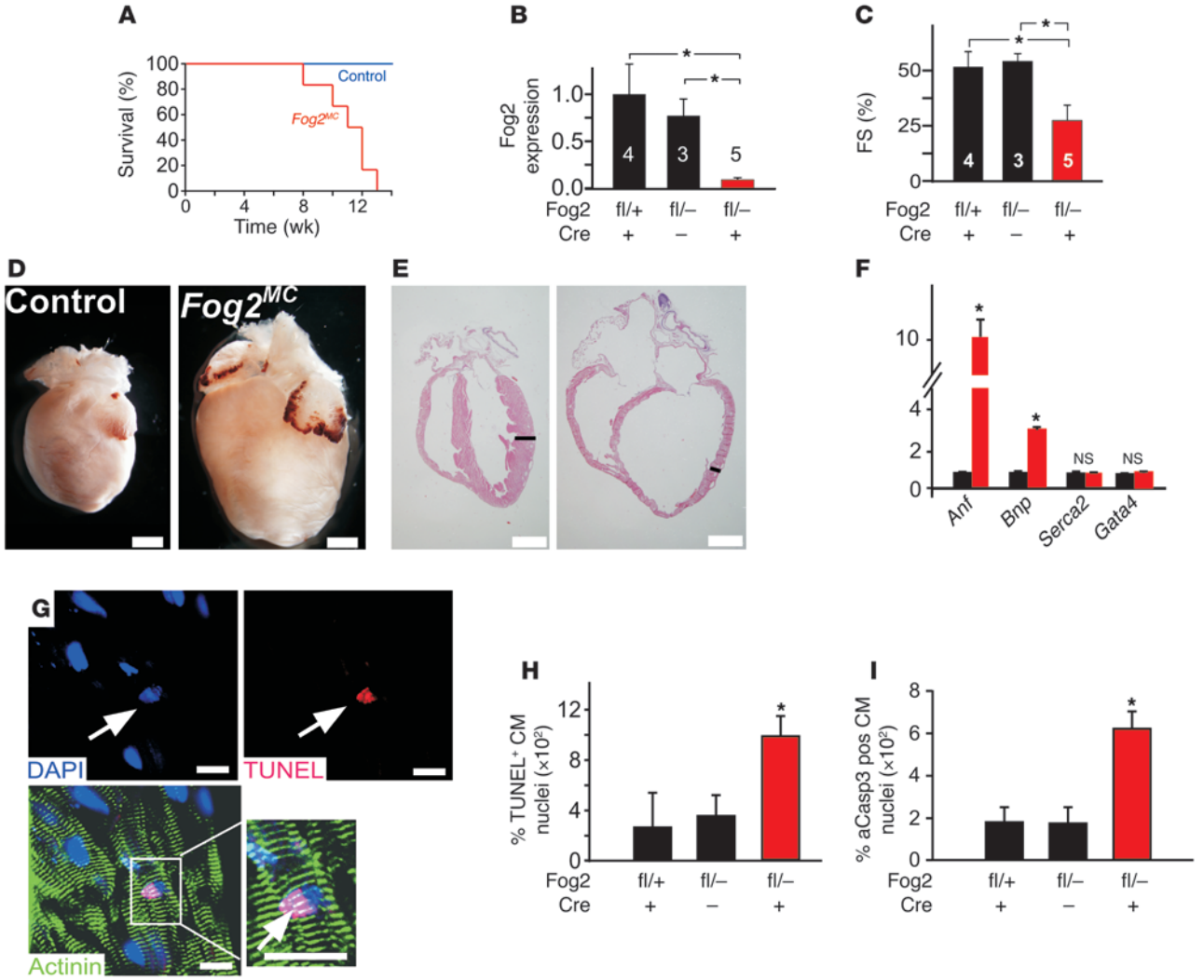

Figure 4

Loss of *Fog2* leads to postnatal heart failure. (**A**) Kaplan-Meier survival curve of $Fog2^{MC}$ animals ($n = 6$ per group). (**B**) qRT-PCR showed efficient *Fog2* knockout. (**C**) M-mode measurement of ventricular function in $Fog2^{MC}$ and littermate Cre-nontransgenic control ($Fog2^{fl/-}NTg$). Fractional shortening (FS) was markedly reduced in $Fog2^{MC}$ compared with controls. (**D** and **E**) Gross view and sections of $Fog2^{MC}$ and littermate control $Fog2^{fl/-}NTg$ hearts, indicating dilated cardiomyopathy. The black bar indicates the compact myocardium. Scale bar: 2 mm. (**F**) qRT-PCR of heart failure–related genes in $Fog2^{MC}$ (red bars) and control (black bars). $n = 8$. (**G**) Representative TUNEL staining of $Fog2^{MC}$ heart section. Cardiomyocytes were identified by actinin staining. Arrows indicates apoptotic cardiomyocytes. The apoptotic cardiomyocyte in boxed region is magnified (lower-right panel). Scale bar: 10 μm. (**H**) Quantitation of $TUNEL^+$ cardiomyocytes ($n = 3$ hearts per group). (**I**) Quantitation of activated caspase-3^+ (aCasp3) cardiomyocytes (CM) ($n = 3$ hearts per group). $^*P < 0.05$.

Cardiomyocyte-restricted *Fog2* inactivation induced in adulthood impaired cardiac systolic function, as indicated by significantly diminished fractional shortening in $Fog2^{iCre–Dox}$ hearts compared with $Fog2^{iCre–Ctrl}$ hearts ($P < 0.001$; Table 2 and Figure 6C). This effect was not due to Dox treatment itself, as Dox did not affect systolic function of $Fog2^{fl/fl}NTg$ hearts (Figure 6C). To further confirm the relationship between reduced *Fog2* expression and heart function, we monitored $Fog2^{iCre}$ and control mice after Dox treatment for 0, 4, 8, 14, and 21 days. Both *Fog2* expression and fractional shortening progressively decreased in $Fog2^{iCre}$ mice over the course of the study, with decrease in *Fog2* expression appearing to precede cardiac dysfunction by approximately 1 week (Figure 6, D and E; e.g., compare days 14 and 21). Consistent with our findings in $Fog2^{MC}$ mice, cardiac dysfunction in $Fog2^{iCre–Dox}$ mice was not associated with significant changes in cardiomyocyte sarcomeric or mitochondrial structure (Figure 6F).

As in $Fog2^{MC}$ mice, PECAM staining of $Fog2^{iCre–Dox}$ tissue demonstrated diminished coronary vascular density (Figure 6, G and H). Consistent with this, Microfil injection suggested that the coronary vasculature was less extensive in $Fog2^{iCre–Dox}$ mice compared with $Fog2^{iCre–Ctrl}$ mice (data not shown). Decreased coronary vascular density was associated with increased apoptosis of $Fog2^{iCre–Dox}$ endothelial cells, as demonstrated by both TUNEL and activated caspase-3 staining (Figure 6I and data not shown). Cardiomyocyte apoptosis likewise increased in $Fog2^{iCre–Dox}$ hearts (Figure 6J), suggesting that increased cardiomyocyte loss contributed to impair-

Table 2
Echocardiographic parameters

Conditional genotype	Cre	Dox	LVEDD	LVESD	LVPWth	FS (%)	HR
Fog2$^{fl/WT}$	*NTg*		2.95 ± 0.13	1.53 ± 0.31	0.41 ± 0.06	48.4 ± 7.8	689 ± 31
Fog2$^{fl/WT}$	*Mhy6-Cre*		3.09 ± 0.33	1.39 ± 0.55	0.42 ± 0.16	54.5 ± 7	727 ± 55
Fog2$^{fl/\Delta}$	*NTg*		2.92 ± 0.21	1.33 ± 0.47	0.44 ± 0.04	54.2 ± 3.3	733 ± 47
Fog2$^{fl/\Delta}$	*Mhy6-Cre*		3.6 ± 0.22	2.61 ± 0.34^{A}	0.32 ± 0.06^{B}	27.5 ± 7^{C}	699 ± 28
Fog2$^{fl/fl}$	*NTg*	–	3.27 ± 0.37	1.61 ± 0.03	0.47 ± 0.12	50.3 ± 6.6	717 ± 72
Fog2$^{fl/fl}$	*iTNT-Cre*	–	3.07 ± 0.07	1.41 ± 0.18	0.48 ± 0.06	54.2 ± 5.6	660 ± 54
Fog2$^{fl/fl}$	*NTg*	+	2.94 ± 0.17	1.39 ± 0.21	0.45 ± 0.06	53.0 ± 4.8	629 ± 64
Fog2$^{fl/fl}$	*iTNT-Cre*	+	3.58 ± 0.58	2.82 ± 1.02^{A}	0.41 ± 0.10	23.2 ± 18.2^{C}	608 ± 51
Gata4$^{fl/WT}$	*NTg*		2.75 ± 0.4	1.36 ± 0.19	0.67 ± 0.07	49.7 ± 1.8	640 ± 51
Gata4$^{fl/ki}$	*Mhy6-Cre*		3.37 ± 0.43	1.42 ± 0.24	0.64 ± 0.08	46.4 ± 7.4	617 ± 45
Gata4$^{fl/WT}$	*NTg*		3.06 ± 0.18	1.36 ± 0.14	0.68 ± 0.09	50.4 ± 1.9	587 ± 71
Gata4$^{fl/ki}$	*Mhy6-Cre*		3.9 ± 0.33	2.62 ± 0.23^{A}	0.46 ± 0.06^{B}	25.7 ± 6.5^{C}	641 ± 59

In the Dox column, + indicates Dox treatment and – indicates no Dox treatment. Fl, floxed allele; WT, WT allele; Δ, null allele; *ki*, Gata4 point mutant allele; NTg, nontransgenic; LVEDD, LV end diastolic diameter; LVESD, LV end systolic diameter; LVPWth, LV posterior wall thickness; FS, fractional shortening; HR, heart rate. For each group, $n = 3–7$. $^{A}P < 0.001$, $^{B}P < 0.05$, $^{C}P < 0.001$ compared with controls.

ment of systolic function. In keeping with increased cardiomyocyte loss, more fibrosis was also noticed in *Fog2*$^{iCre–Dox}$ hearts compared with *Fog2*$^{iCre–Ctrl}$ hearts (Figure 6K). Collectively, these data demonstrated that *Fog2* expression in adult cardiomyocytes is necessary to maintain heart function and coronary vasculature.

Block of FOG2-GATA4 interaction resulted in postnatal heart failure. Given the requirement of GATA4 for normal function of the adult heart (7, 8) and the requirement of GATA4-FOG interaction for heart development (13), we hypothesized that FOG2 action in the adult heart is mediated by interaction with GATA4. To test this hypothesis, we used a conditional complementation approach. We complemented *Gata4*^{ki}, a missense *Gata4* allele encoding a GATA4[V217G] protein specifically deficient in FOG2 interaction (13), with *Gata4*^{fl}, a floxed *Gata4* allele. In embryo heart, Cre-recombined *Gata4*^{fl} produced a functionally inactivate, truncated GATA4 protein (2), while in adult heart, it did not express detectable protein (7). Thus, in *Gata4*$^{fl/ki}$*Cre*$^{+}$ embryos, GATA4[V217G] is the sole full-length GATA4 protein within the Cre recombination domain.

We generated *Gata4*$^{fl/ki}$*Nkx2-5*$^{Cre/+}$ (*Gata4*$^{ki–NK}$) and *Gata4*$^{fl/ki}$*Myh6-Cre* (*Gata4*$^{ki–MC}$) embryos. *Nkx2-5*$^{Cre/+}$ and *Myh6-Cre* efficiently inactivated *Gata4*^{fl} by E9.5 and E12.5, respectively (6). Early loss of GATA4-FOG2 interaction in *Gata4*$^{ki–NK}$ embryos resulted in edema and peripheral hemorrhage, consistent with heart failure (Supplemental Figure 9A). Morphologically, *Gata4*$^{ki–NK}$ embryos developed a spectrum of cardiac defects similar to those seen in *Fog2*^{NK} embryos: thin compact myocardium, AV cushion defect, VSD, and impaired coronary vascular development (Supplemental Figure 9, B–D). Importantly, *Gata4*$^{fl/+}$*Nkx2-5*$^{Cre/+}$ embryos developed normally, suggesting that the phenotype of *Gata4*$^{ki–NK}$ embryos is not due to *Gata4* or *Nkx2-5* haploinsufficiency. These data strongly indicated that FOG2-GATA4 interaction in cardiomyocytes is critical for cardiac morphogenesis and coronary vascular development.

As in *Fog2*^{MC} mice, later ablation of FOG2-GATA4 interaction in *Gata4*$^{ki–MC}$ embryos was compatible with normal survival to term but caused severely diminished systolic function at 8–14 weeks as shown by echocardiography and PET imaging (Figure 7A, Table 2, and Supplemental Videos 3 and 4). This was not due to haploinsufficiency for either GATA4 or GATA4-FOG2 interaction, as controls with *Gata4*$^{fl/+}$*Myh6-Cre* and *Gata4*$^{fl/ki}$*NTg* genotypes had normal systolic function (Figure 7A and Table 2). Histological analysis showed ventricular dilatation and fibrosis (Supplemental Figure 10, E and F). Consistent with heart failure, *Anf* and *Bnp* mRNAs were significantly upregulated (Supplemental Figure 9G). *Serca2* expression was unchanged (Supplemental Figure 9, G and H). *Fog2* expression was also unchanged, indicating that the *Gata4*$^{ki–MC}$ phenotype was not secondary to epistasis between *Gata4* and *Fog2*.

Cardiomyocyte and endothelial cell apoptosis were significantly increased in *Gata4*$^{ki–MC}$ mutants compared with controls (Figure 7, B and C). Injection of Microfil revealed that the coronary vasculature of *Gata4*$^{ki–MC}$ hearts was dramatically diminished, suggesting impaired myocardial perfusion in *Gata4*$^{ki–MC}$ hearts (Figure 7D). Consistent with these data and the *Fog2*^{MC} phenotype, *Gata4*$^{ki–MC}$ hearts had reduced coronary capillary and arteriolar density compared with control hearts, as determined by quantitative analysis of PECAM- and SMA-stained sections ($P < 0.05$; Figure 7, E and F). Cardiac fibrosis was also increased in *Gata4*$^{ki–MC}$ (Figure 7G). Together, these data indicate that FOG2-GATA4 interaction is critical for postnatal cardiac function and maintenance of coronary vasculature.

Regulation of a proangiogenic gene program by Fog2. To pursue the molecular mediators of *Fog2* action in the postnatal heart, we used microarrays to compare gene expression in 6-week-old *Fog2*^{MC} and control (*Fog2*$^{fl/–}$*NTg*) heart ventricles ($n = 3$ per group). Six hundred and forty genes were differentially expressed ($P < 0.005$), with 248 downregulated and 392 upregulated. Among these genes were *Fog2* itself and *Anp* and *Bnp*, findings that were supported by qRT-PCR (Figure 4, B and F). Additional intriguing dysregulated genes were cardiotrophin 1 (*Ctf1*; downregulated), the potassium voltage-gated channel, Isk-related family, member 1 (*Kcne1*, also known as *MinK*; upregulated), *Ppara* (downregulated), and the forkhead box C1 (*Foxc1*; upregulated). We measured these by qRT-PCR, and confirmed altered expression of all except *Ppara*. KCNE1 is an essential subunit of the cardiac slow delayed rectifier (I_{Ks}) channel, which contributes to cardiac repolarization. Although *Kcne1* mRNA was dramatically upregulated, we did not observe arrhythmia or altered electrocardiographic parameters in *Fog2*^{MC} mice (Supplemental Table 1 and data not shown). Altered expression of *Ctf1* and *Foxc1* may contribute directly to cardiomyocyte dysfunction or apoptosis in *Fog2*^{MC} hearts (see Discussion).

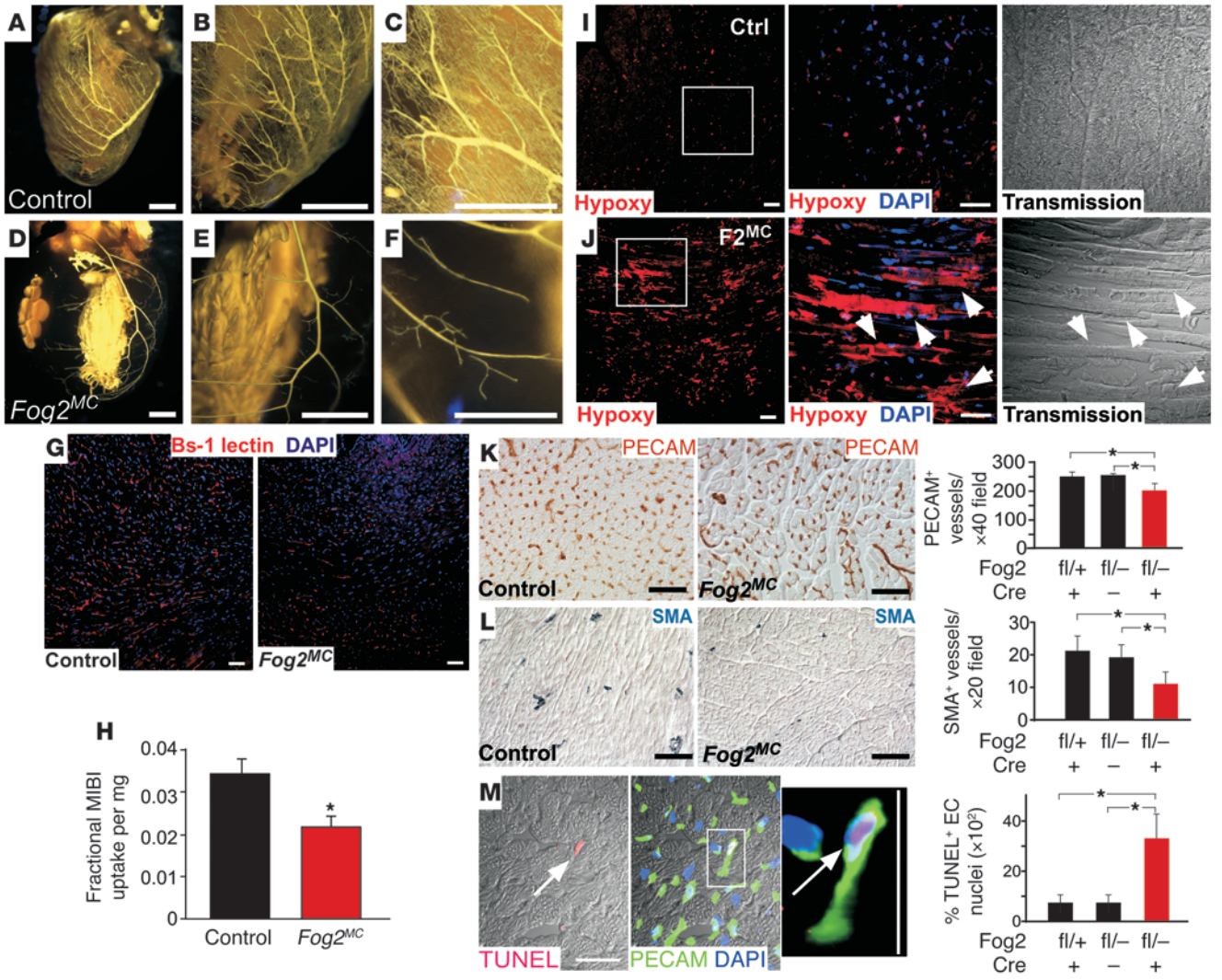

Figure 5

Defective myocardial perfusion and coronary vasculature in adult *Fog2*^{MC} heart. (**A**–**F**) Cleared, Microfil-injected control and *Fog2*^{MC} hearts. Microvascular filling by Microfil was markedly reduced in *Fog2*^{MC} hearts compared with control. (**G**) Perfusion labeling of endothelial cells by injected Bs-1 lectin. Myocardial labeling was reduced in *Fog2*^{MC}. (**H**) Assessment of myocardial perfusion by myocardial MIBI uptake. Uptake is expressed as a fraction of the injected dose, normalized to heart weight. (**I** and **J**) Representative figure of hypoxia in *Fog2*^{MC} myocardium. Hypoxia was detected as immunoreactivity to hypoxyprobe (hypoxy). Staining was greater in *Fog2*^{MC} myocardium, including cardiomyocytes (arrowheads). Boxed regions are magnified in center panels. Transmission" indicates phase-contrast images. (**K**) Decreased capillary density in *Fog2*^{MC} myocardium. PECAM^{+} vessels in histological sections were quantitated. (**L**) Decreased smooth muscle–positive vessels in *Fog2*^{MC} myocardium. (**M**) Increased endothelial cell apoptosis in *Fog2*^{MC} myocardium. The boxed apoptotic endothelial cell is magnified (right panel). Apoptosis was quantitated by TUNEL staining of PECAM^{+} coronary endothelial cells (white arrow). For quantitation in **H** and **K**–**M**, n = 3–4 for each group. *P < 0.05. Scale bar: 500 μm (**A**, **B**, **D**, and **E**); 250 μm (**C** and **F**); 50 μm (**G** and **I**–**M**).

Few angiogenesis-related genes were uncovered in our microarray screen. However, at a sample size of 3, our microarray screen lacked statistical power to detect many important biological changes. Therefore, we assembled a list of angiogenesis-related genes from the literature, and examined the microarray data for suggestive gene expression changes. We then directly measured expression of 17 angiogenic factors with suggestive microarray changes by qRT-PCR, comparing *Fog2*^{MC} with controls with sample sizes increased to 8 per group. Expression of 14 of these angiogenesis-related genes was altered (Figure 8A). The proangiogenic genes *Vegfa*, *Fgf2*, *Fgf9*, *Fgf12*, and *Fgf16* were significantly downregulated, while the angiogenesis inhibitors thrombospondin 1 (*Thbs*), tissue inhibitor of metalloproteinase 1 (*Timp1*), *Timp2*, heparanase (*Hpse*), and collagen, type IV, α 3 (*Col4a3*), collagen, type XV, α 1 (*Col15a*), and collagen, type XVIII, α 1 (*Col18a*) were upregulated. Next, we asked whether FOG2 acts through GATA4 to regulate these genes. We compared expression of these same genes between *Gata4*$^{ki–MC}$ and control hearts (n = 7–9 per group). Expression of nearly all of these genes was also disrupted in *Gata4*$^{ki–MC}$, and the direction of change was concordant with that observed in *Fog2*^{MC} (Figure 8B). These data indicate that a FOG2-GATA4 complex coordinates expression of a set of pro- and antiangiogenesis genes, acting to promote an overall proangiogenic gene expression profile.

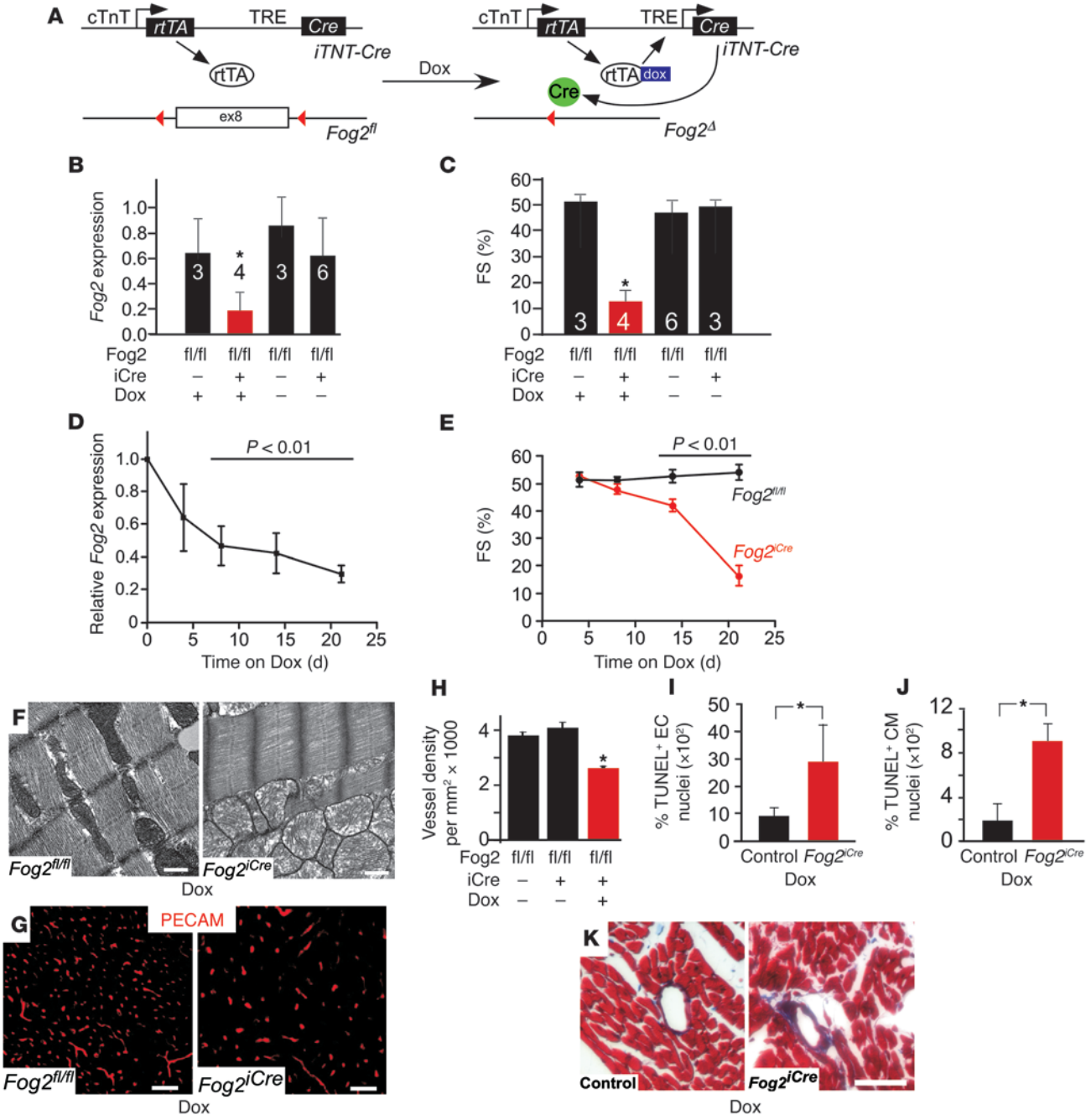

Figure 6

Postnatal inactivation of Fog2 caused cardiac failure. (**A**) *Fog2* inactivation strategy in adult mice. cTnT, cardiac troponin T promoter; ex8, *Fog2* exon 8; $Fog2^{\Delta}$, Cre-inactivated Fog2 allele; rtTA, reverse tet activator protein; TRE, tet activator protein response element. Red triangles indicate loxP sites. (**B**) Decreased *Fog2* expression in Dox-treated $Fog2^{iCre}$ heart apexes compared with controls. (**C**) Decreased ventricular function in $Fog2^{iCre}$ mice after 4 weeks of Dox treatment. (**D** and **E**) Time course of *Fog2* inactivation and ventricular systolic function during Dox treatment. Fog2 expression was determined by qRT-PCR ($n = 4$ per time point). (**F**) Electron microscopy showed that sarcomere and mitochondrial structures were well preserved in $Fog2^{iCre–Dox}$ mutant hearts. Scale bar: 500 nm. (**G** and **H**) PECAM (red) staining showed decreased density of coronary blood vessels in $Fog2^{iCre–Dox}$ hearts compared with those of controls. $n = 3$ per group. Scale bar: 50 μm. (**I** and **J**) Quantitation of $TUNEL^{+}$ coronary endothelial cells (ECs) and cardiomyocytes. Apoptosis increased in $Fog2^{iCre–Dox}$ hearts compared with those of $Fog2^{fl/fl}$ littermate controls. $n = 3$ per group. (**K**) Trichrome staining demonstrating increased fibrotic tissues in $Fog2^{iCre–Dox}$ hearts. Scale bar: 50 μm. $^{*}P < 0.05$.

Coordination of cardiac growth and angiogenesis is in part mediated by the secretion of angiogenic growth factors from myocytes (28). The abnormal expression profile of angiogenesis-related genes suggested that *Fog2*-deficient cardiomyocytes were defective in their ability to support endothelial growth and vessel formation. To further investigate the functional role of cardio-

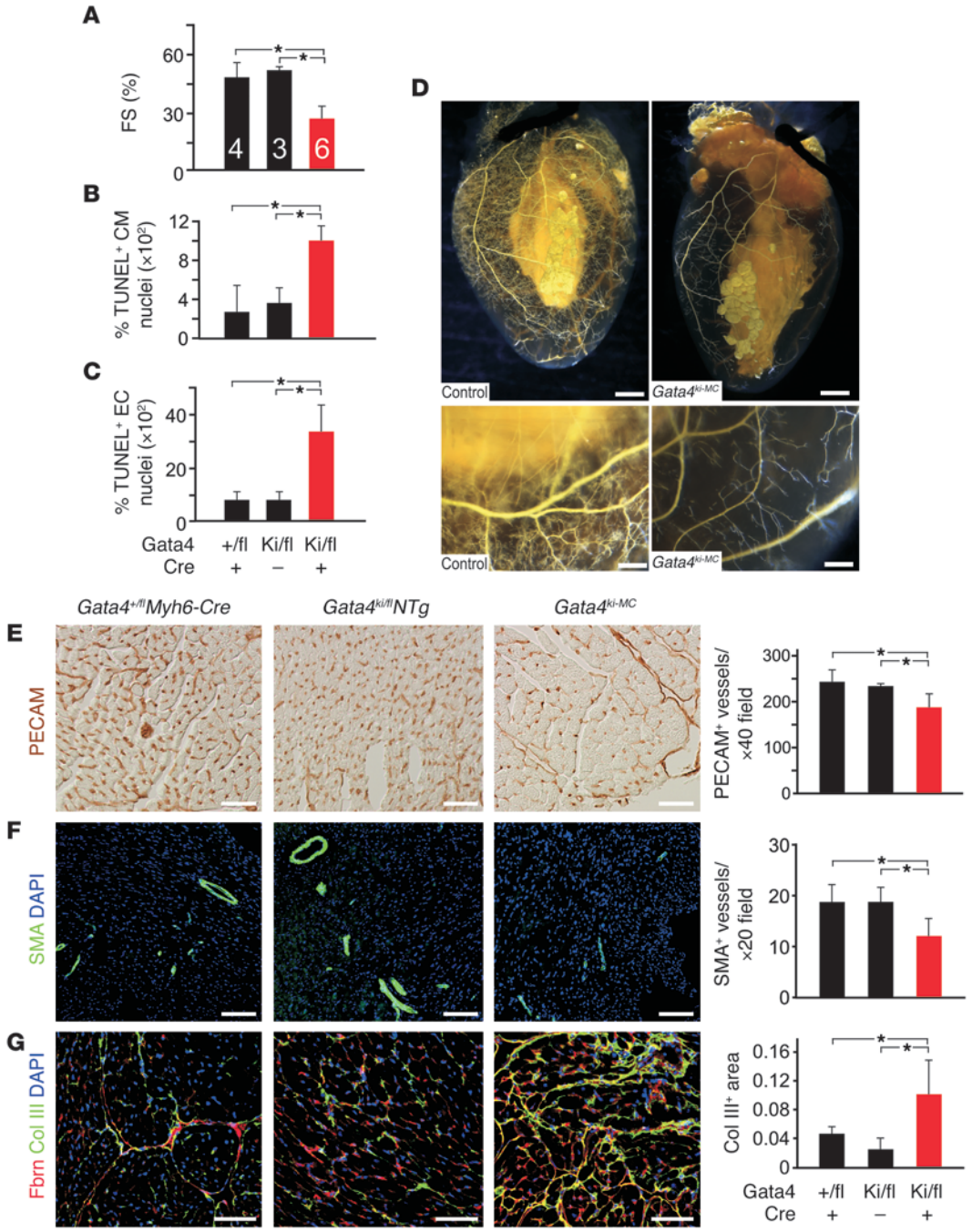

Figure 7
Heart failure due to disruption of FOG2-GATA4 interaction. (**A**) Severely decreased heart function in *Gata4*$^{ki–MC}$ mice compared with *Gata4*$^{fl/+}$*Myh6-Cre* or *Gata4*$^{fl/ki}$*NTg*. (**B** and **C**) Quantitation of TUNEL$^+$ cardiomyocytes and coronary endothelial cells showed increased apoptosis in *Gata4*$^{ki–MC}$ hearts compared with those of controls (n = 3 per group). (**D**) Injected Microfil demonstrated reduced coronary microvasculature in *Gata4*$^{ki–MC}$ hearts compared with littermate control (*Gata4*$^{+/fl}$ *Myh6-Cre*). Scale bar: 1 mm (top panels); 200 μm (bottom panels). (**E**) PECAM staining revealed decreased capillary density in *Gata4*$^{ki–MC}$ hearts compared with controls (n = 3). (**F**) SMA staining revealed decreased arteriole density in *Gata4*$^{ki–MC}$ hearts compared with controls (n = 3). (**G**) Fibronectin and collagen III (Col III) staining revealed significantly increased fibrosis in *Gata4*$^{ki–MC}$ hearts compared with controls (n = 3). Scale bar: 100 μm. *P < 0.05.

myocyte FOG2 in regulating angiogenesis, we used an in vitro cardiomyocyte–endothelial cell coculture system. Primary neonatal *Fog2*$^{fl/fl}$ cardiomyocytes were cultured on matrigel and treated with adenovirus expressing either Cre or LacZ (negative control). Cre adenovirus efficiently reduced Fog2 expression (Figure 8, C and D). Next, we plated HUVECs on the cardiomyocytes and assessed tubule formation. The quality and quantity of tubule formation was significantly decreased by cardiomyocyte inactivation of *Fog2* (Figure 8, E and F), suggesting that *Fog2* regulates a proangiogenic gene program in cardiomyocytes that promotes capillary-like structure formation. In addition, we asked whether cardiomyocyte Fog2 regulates endothelial cell proliferation. Cardiomyocyte Fog2 inactivation decreased HUVEC BrdU incorporation (Figure 8, G and H), indicating that *Fog2* regulates the expression of cardiomyocyte-secreted factors that stimulate endothelial cell proliferation.

In summary, we performed temporal and spatial inactivation of *Fog2* in embryos and found early, but not late, requirement of FOG2 expression and FOG2-GATA4 interaction for cardiac morphogenesis and coronary vasculogenesis. In addition, maintenance of postnatal heart function also required FOG2 and its interaction with GATA4. *Fog2* regulates a subset of angiogenesis-related genes, and loss of *Fog2* caused decreased coronary vasculature and tissue hypoxia, which subsequently resulted in cardiomyocyte cell death and heart failure.

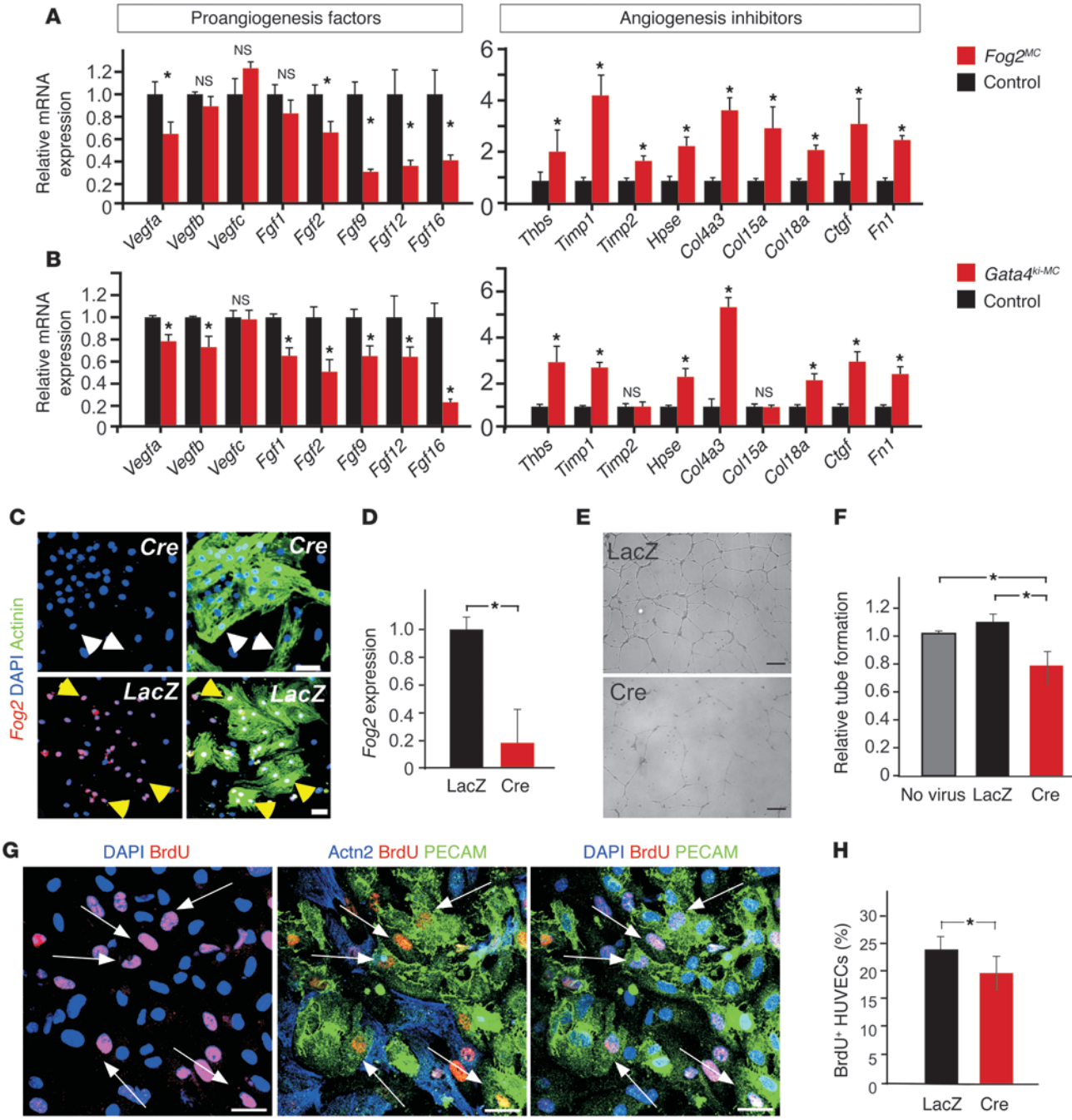

Figure 8

Fog2 regulation of angiogenesis. (**A**) Relative expression of genes encoding secreted angiogenesis-related factors in *Fog2*^{MC} heart apex compared with controls. Gene expression was measured by qRT-PCR. $n = 8$ per group. *Thbs*, thrombospondin 1; *Timp1*, tissue inhibitor of metalloproteinase 1; *Hpse*, heparanase; *Col4a3*, collagen, type IV, α 3; *Col15a*, collagen, type XV, α 1; *Col18a*, collagen, type XVIII, α 1; *Ctgf*, connective tissue growth factor; *Fn1*, fibronectin 1. (**B**) Relative expression of genes encoding secreted angiogenesis-related factors in *Gata4*$^{ki-MC}$ heart apex ($n = 7$) compared with controls ($n = 9$). (**C**) Depletion of *Fog2* in cultured mouse neonatal cardiomyocytes. *Fog2*$^{fl/fl}$ cardiomyocytes treated with Cre adenovirus showed reduced FOG2 immunoreactivity (white arrowheads), while FOG2 was readily detected after treatment with control LacZ adenovirus (yellow arrowheads). (**D**) Relative expression of *Fog2*, as assessed by qRT-PCR. Cre strongly reduced *Fog2* expression compared with LacZ. (**E**) Representative images of tubule formation by HUVECs plated on matrigel and cocultured with Cre or LacZ virus–treated *Fog2*$^{fl/fl}$ cardiomyocytes. (**F**) *Fog2*$^{fl/fl}$ cardiomyocytes stimulated less HUVEC tubule formation after Cre treatment than after LacZ treatment. $n = 3$. (**G**) BrdU staining of PECAM$^+$ HUVECs cocultured with cardiomyocytes (sarcomeric α actinin [Actn2]). Scale bar: 20 μm. (**H**) The percentage of BrdU$^+$ cells in HUVECs cocultured with *Fog2*$^{fl/fl}$ cardiomyocytes that have been treated with Cre or LacZ adenovirus ($n = 5$). $^*P < 0.05$.

Discussion

A conserved transcriptional network regulates development and function of the heart from embryogenesis through adulthood by regulating the expression of key downstream genes. Understanding the function of members of this transcriptional network is therefore an important strategy for gaining insights into molecular pathways that underlie congenital and acquired heart disease. In this work, we investigated the role of *Fog2* in the developing and adult heart, using a spatiotemporal conditional gene inactivation strategy. Myocardial FOG2 interaction with GATA4 was required for cardiac morphogenesis and development of the coronary vascular plexus and also for normal adult heart function and maintenance of coronary vasculature. FOG2 and GATA4 jointly promoted coronary angiogenesis by coordinating the expression of a proangiogenic gene program.

Role of FOG2 in heart development. *Fog2* is expressed in the myocardial, epicardial, and endocardial layers of the developing heart. Germline *Fog2* deletion resulted in severe abnormalities of myocardial growth, endocardial cushion development, and coronary vascular development. In this work, we dissected the requirement of *Fog2* in myocardial, epicardial, and endocardial compartments for each of these aspects of heart development.

We determined that FOG2 and FOG2-GATA4 interaction were required in a cell autonomous manner in cardiomyocytes prior to E12.5 for myocardial growth, as demonstrated by disruption of this process in $Fog2^{NK}$ and $Gata4^{ki–NK}$ mutants. A preponderance of FOG2 activities appeared to require GATA4 (as indicated by the phenotypic similarities of these mutants). After E12.5, embryonic growth and morphogenesis of the heart did not appear to require *Fog2*, as demonstrated by normal heart structure and morphogenesis of $Fog2^{MC}$ and $Gata4^{ki–MC}$ mutant embryos and neonates.

Interestingly, epicardial *Fog2* also appeared to promote growth of the compact myocardium, as some $Fog2^{fl/–}Wt1^{GFPCre/+}$ embryos had severe thinning of the compact myocardium. Loss of *Fog2* in epicardium likely disrupts epicardial-myocardial cross-talk that is essential for expansion of the compact myocardium (20, 29). Paracrine factors, such as FGFs, erythropoietin, Wnts, and retinoic acid are known to drive normal growth of the compact myocardium (30–32), suggesting that a subset of these factors may lie downstream of epicardial *Fog2*.

Development of the AV endocardial cushions requires FOG2, as shown by the severe AV endocardial cushion defects observed in $Fog2^{–/–}$ mutants. Interestingly, this *Fog2* requirement does not reflect a cell autonomous function of *Fog2* in endocardial cells or their derivatives, as $Fog2^{T2}$ hearts were structurally normal. A cell autonomous function of *Fog2* in the *Tie2Cre* recombination domain may be masked by functional redundancy with *Fog1*, which is required in the endocardium, and its derivatives for endocardial cushion development (21). However, *Fog2* was required in myocardial cells for normal endocardial cushion development, as myocardial-restricted inactivation of *Fog2* by $Nkx2\text{-}5^{Cre}$ resulted in endocardial cushion defects similar to those seen in $Fog2^{–/–}$ hearts, which have been linked to human tricuspid atresia (10). Finally, we found that epicardial inactivation of *Fog2* also caused endocardial cushion defects. EPDCs have been described to contribute to AV cushion mesenchyme (23), but to our knowledge epicardial-restricted gene mutation has not been previously shown to disturb development of AV endocardial cushions.

Role of FOG2 in maintenance of adult heart function. Our data showed that FOG2 and its interaction with GATA4 are essential for normal adult heart function. While developmental defects may contribute to the overall $Fog2^{MC}$ and $Gata4^{ki–MC}$ phenotypes, significant cardiac dysfunction and reduced coronary vessel density in the $Fog2^{iCre–Dox}$ adult inactivation model clearly demonstrate a continuing requirement for *Fog2* in the adult heart ($P < 0.001$; Table 2). Most of the known functions of FOG proteins require interaction with GATA family proteins (12). Our experiments extend the functional significance of FOG2-GATA4 interaction into the adult heart, in which it is essential to maintain heart function and coronary vasculature.

Pathogenesis of heart failure in mutants lacking adult cardiomyocyte FOG2 or FOG2-GATA4 interaction is likely multifactorial. Cardiomyocyte apoptosis increased in all 3 adult mutant models that we examined. Although the frequency of apoptotic cardiomyocytes was low (roughly 1 in 1,000 in $Fog2^{MC}$), the cumulative effect of this level of apoptosis was sufficient to cause heart failure in other models (26, 27). Diminished cardiomyocyte perfusion and cardiomyocyte hypoxia almost certainly contributed to increased cardiomyocyte apoptosis (see below). However, cardiomyocyte gene expression changes may also directly contribute. In $Fog2^{MC}$ hearts, *Ctf1* expression was downregulated. *Ctf1* encodes a cardiomyocyte survival factor that signals through the gp130 receptor. Loss of gp130 receptor signaling sensitized the heart to load-induced cardiomyocyte apoptosis and heart failure (33).

Other gene expression changes downstream of FOG2 or FOG2-GATA4 interaction likely directly influenced cardiomyocyte function. The transcription factor gene *Foxc1* was significantly ($P < 0.005$) upregulated in both $Fog2^{MC}$ and $Gata4^{ki–MC}$ models. The FOX transcription factor binding motif was significantly enriched among genes differentially expressed in human and murine heart failure (34), suggesting that members of this family participate in heart failure pathogenesis. Within the FOX family, *Foxc1* was among the most highly expressed in the adult heart (34). Thus, increased expression of *Foxc1* may contribute to gene dysregulation and altered heart function in $Fog2^{MC}$ and $Gata4^{ki–MC}$ models.

Kcne1, essential for the I_{Ks} repolarization current, was upregulated 4- to 10-fold in both $Fog2^{MC}$ and $Gata4^{ki–MC}$ mutants. *Kcne1* mutation causes human long QT syndrome, characterized by prolonged ventricular repolarization and susceptibility to lethal ventricular arrhythmia. Interestingly, the *Kcne1* promoter contains GATA binding sites that are required for full activity (35), suggesting that FOG2-GATA4 directly modulates *Kcne1* expression. Although we did not identify differences in cardiac impulse conduction or repolarization in $Fog2^{MC}$ electrocardiograms, aberrant *Kcne1* expression may contribute to the predisposition of the failing heart to arrhythmia.

Role of FOG2 in coronary vascular development and maintenance. In the developing heart, $Fog2^{–/–}$ and $Gata4^{ki/ki}$ mutant mice are defective for formation of the coronary vascular plexus. We showed that the coronary vascular requirement for *Fog2* is restricted to cardiomyocytes prior to E12.5. While it was previously hypothesized that the coronary vessel defect of *Fog2*-null mutant mice was due to defective epicardial EMT, we explicitly tested this hypothesis and found that epicardial EMT was intact in *Fog2*-null mice. Moreover, lineage tracing experiments in mice using 3 different epicardial-restricted Cre alleles — $Wt1^{GFPCre}$ (19), T-box 18 ($Tbx18^{Cre}$) (36), and a chicken *Gata5* enhancer driven Cre transgene (32) — demonstrated that only a small minority or none of endothelial cells originate from the epicardium in mouse. The origin of the majority of coronary endothelial cells still remains uncertain. Thus, defective formation of the vascular endothelial plexus in *Fog2* mutant mice is unlikely to be due to impaired epicardial EMT.

In adult heart, the coronary vessels supply oxygen and nutrients to metabolically active cardiomyocytes. Impaired myocardial perfusion leads to tissue hypoxia, diminished cardiomyocyte performance, increased cardiomyocyte apoptosis, and ultimately, heart failure. Loss of *Fog2* or FOG2-GATA4 interaction impaired myocardial perfusion. Interestingly, the functional perfusion defect appeared greater than the measured decrease in capillary and arteriole density. Thus, in addition to these structural changes, myocardial perfusion may have also diminished as a result of decreased connectivity among endothelial cells or as a result of dynamic factors, such as coronary vasospasm. Interestingly, connections between endothelial tubules were reduced by *Fog2* inactivation in the vascular tubule formation assay, which is somewhat reminiscent of establishment of capillary connectivity in vivo.

Myocardial *Gata4* was previously implicated in promoting angiogenesis by stimulating VEGF secretion (9). Our work extends this finding in several ways. First, we demonstrated the importance of FOG2 and its interaction with GATA4 in promoting angiogenesis. Second, the induced adult inactivation of *Fog2* clearly demonstrated a cause-effect relationship between adult *Fog2* loss-of-function and vascular abnormalities in the adult heart. Third, we showed that FOG2 and GATA4 regulate a broad panel of angiogenesis-related genes, coordinating their expression to promote angiogenesis.

Vascular homeostasis is a complex process that includes growth of new vessels and maintenance of the existing vessels. Both of these processes are orchestrated by a myriad of angiogenic factors and inhibitors, imbalance of which contributes to tissue ischemia and other pathological conditions (37). A number of angiogenesis-related factors were differentially expressed in the $Fog2^{MC}$ and $Gata4^{ki–MC}$ models. Altered expression of these factors was coordinated, so that the direction of change of each factor in the mutants tended to inhibit angiogenesis. Thus, angiogenic genes (*Vegfa*, *Vegfb*, *Fgf1*, *Fgf2*, *Fgf9*, *Fgf12*, and *Fgf16*) were downregulated, and angiostatic genes (*Thbs*, *Timp1*, *Timp2*, *Hpse*, *Col4a3*, *Col15a*, *Col18a*, connective tissue growth factor [*Ctgf*], and fibronectin 1 [*Fn1*]) were upregulated. Further studies are required to understand the regulation of these genes downstream of FOG2-GATA4. It will be important to define which genes are direct regulatory targets and which genes are regulated indirectly through other factors. One major target of FOG2-GATA4 is *Vegfa*, which was shown by Heineke et al. to be directly regulated by GATA4 (9). FGFs are also potent proangiogenic factors (38), and in other systems, *Fgfs* are regulated by FOG and GATA (reviewed in ref. 29). The regulatory relationships are likely complex, as VEGFs and FGFs stimulate each other's expression and potentiate each other's angiogenic activity (39–41).

Several angiogenesis inhibitors were substantially increased in $Fog2^{MC}$ and $Gata4^{ki–MC}$. Tissue inhibitors of metalloproteinases provide critical extracellular regulation of the proteolytic activities of MMPs and abrogate angiogenic factor-induced endothelial cell proliferation in vitro and angiogenesis in vivo (37). *Timp1* and *Timp2* levels increased in our models, which would negatively impact coronary angiogenesis. Proteolytic degradation of collagens encoded by *Col18a1* and *Col4a3* yield the potent endogenous angiogenesis inhibitors endostatin and tumstatin, respectively. Both of these genes were substantially upregulated in $Fog2^{MC}$ and $Gata4^{ki–MC}$ mutant hearts. Endostatin and tumstatin are broad spectrum angiogenesis inhibitors being investigated as anticancer agents because of their powerful angiogenesis blocking activity (42). Tumstatin induced HUVEC apoptosis and inhibited FGF-stimulated HUVEC proliferation (43). *Col15a1*, upregulated in our models, regulates endothelial survival and capillary formation in heart and encodes an endostatin-like peptide with antiangiogenic activities (44). Our studies suggest the intriguing hypothesis that altered expression of these endogenous collagen genes may influence coronary vascular density in human heart failure.

In summary, we have delineated the tissue-specific requirements for FOG2 in heart development and demonstrated that cardiomyocyte-restricted FOG2 acts through GATA4 to regulate heart morphogenesis, heart function, and establishment and maintenance of coronary vessels. We have shown that a FOG2-GATA4 complex is required for the coordinate regulation of an angiogenic gene program. Genes downstream of FOG2-GATA4, such as collagens with antiangiogenic properties, may represent novel therapeutic avenues for treatment of human heart disease.

Methods

Animal procedures. Mouse models are described in the Supplemental Methods. All animal experiments were performed according to protocols approved by the Institutional Animal Care and Use Committee of Children's Hospital Boston.

Perfusion assays. After injection of Bs-1 lectin (Vector Laboratories) or hypoxyprobe-1 (NPI Inc.), excised hearts were fixed and processed for immunohistochemistry. For MIBI uptake, the fraction of injected MIBI taken up by the heart was measured by scintillation counting and expressed as the fraction uptake per milligram heart weight. Microfil (Flow Tech Inc.) was prepared as recommended by the manufacturer and injected into the LV after ascending aortic ligation. Hearts were cleared in methyl-salicylate.

Section immunohistochemistry. Immunostaining was performed as described (19, 45). TUNEL (In Situ Cell Death Detection Kit, Roche) staining was performed on cryosections according to manufacturer's instructions. The sources and dilutions of antibodies are provided in Supplemental Methods. Weak signals were amplified with tyramide-Cy3 (PerkinElmer). Images were acquired on a FV1000 confocal microscope (Olympus). Quantitation was performed by a blinded observer.

Whole-mount staining. Whole-mount PECAM staining was performed on E13.5–E14.5 hearts, fixed in zinc fixative (BD Biosciences — Pharmingen), stained with biotinylated PECAM antibody (BD), and developed with the ABC method and DAB chromagen (Vector Laboratories). Coronary coverage was measured by blinded observer on whole-mount images as the ratio of the area covered by coronary vessels to the ventricular area. For X-gal staining, embryos or hearts were stained with 1 mg/ml X-gal at 37°C overnight as described (46).

Gene expression analysis. RNA was extracted with TRIzol (Invitrogen). Affymetrix mouse 430.2 microarrays were hybridized to labeled cRNA and analyzed as described (7) (Gene Expression Omnibus accession number GSE15078). For qRT-PCR, cDNA was amplified on an ABI 7300 Sequence Detector and detected with SYBR Green chemistry (Applied Biosystems). GAPDH was detected with a TaqMan-based assay (Applied Biosystems). Other primer sequences are provided in Supplemental Table 2.

In vitro angiogenesis assays. Neonatal cardiomyocytes ($Fog2^{fl/fl}$), isolated from P1–P2 $Fog2^{fl/fl}$ hearts using the Neomyt kit (Cellutron Inc.), were treated with Cre or LacZ adenovirus. After 2 days, HUVECs were overlaid on the cardiomyocytes and allowed to attach in EGM2 (Cambrex) for 2 hours and then switched to culture media M199 supplemented with 1% penicillin-streptomycin-glutamine (Invitrogen) (no serum). The tubule assay was performed on matrigel (BD Biosciences), using 1×10^5 cardiomyocytes and HUVECs per well. Tubules were measured after 24 hours as described (9). For endothelial cell proliferation, 3×10^4 cardiomyocytes and

HUVECs were plated in gelatin-coated 24-well plates. BrdU was added at 15–21 hours of coculture, and proliferation was measured by staining with BrdU (Sigma-Aldrich) and PECAM antibodies.

Animal physiology. Ventricular function was measured in conscious mice using short axis M-mode images with a VisualSonics Vevo 770 machine. PET was performed using ^{18}F-D-glucose and a Siemens rodent PET system with ECG gating. Standard limb electrocardiograms were recorded with needle electrodes on mice anesthetized with ketamine and xylazine. QT correction was performed as described (47). All physiological measurements were acquired and analyzed by an observer blinded to genotype.

Statistics. Unless otherwise indicated, results are expressed as mean ± SD. Statistical significance was evaluated by Welch's *t* test, using JMP software, version 5.1. *P* values of less than 0.05 were considered to be statistically significant.

Acknowledgments

We thank Patricia Dunning at Animal Core Facility at Children's Hospital Boston for technical assistance. W.T. Pu was supported by a charitable donation from Edward Marram and Karen Carpenter and by a grant from the Harvard Stem Cell Institute. B. Zhou was supported by a grant from the American Heart Association. F.X. McGowan and W.T. Pu were supported by NIH grant P50HL074734.

Received for publication January 27, 2009, and accepted in revised form March 11, 2009.

Address correspondence to: William T. Pu, Enders 1254, Children's Hospital Boston, 300 Longwood Avenue, Boston, Massachusetts 02115, USA. Phone: (617) 919-2091; Fax: (617) 730-0140; E-mail: wpu@enders.tch.harvard.edu.

1. Olson, E.N. 2006. Gene regulatory networks in the evolution and development of the heart. *Science.* **313**:1922–1927.
2. Rivera-Feliciano, J., et al. 2006. Development of heart valves requires Gata4 expression in endothelial-derived cells. *Development.* **133**:3607–3618.
3. Watt, A.J., Battle, M.A., Li, J., and Duncan, S.A. 2004. GATA4 is essential for formation of the proepicardium and regulates cardiogenesis. *Proc. Natl. Acad. Sci. U. S. A.* **101**:12573–12578.
4. Molkentin, J.D., Lin, Q., Duncan, S.A., and Olson, E.N. 1997. Requirement of the transcription factor GATA4 for heart tube formation and ventral morphogenesis. *Genes Dev.* **11**:1061–1072.
5. Kuo, C.T., et al. 1997. GATA4 transcription factor is required for ventral morphogenesis and heart tube formation. *Genes Dev.* **11**:1048–1060.
6. Zeisberg, E.M., et al. 2005. Morphogenesis of the right ventricle requires myocardial expression of Gata4. *J. Clin. Invest.* **115**:1522–1531.
7. Bisping, E., et al. 2006. Gata4 is required for maintenance of postnatal cardiac function and protection from pressure overload-induced heart failure. *Proc. Natl. Acad. Sci. U. S. A.* **103**:14471–14476.
8. Oka, T., et al. 2006. Cardiac-specific deletion of Gata4 reveals its requirement for hypertrophy, compensation, and myocyte viability. *Circ. Res.* **98**:837–845.
9. Heineke, J., et al. 2007. Cardiomyocyte GATA4 functions as a stress-responsive regulator of angiogenesis in the murine heart. *J. Clin. Invest.* **117**:3198–3210.
10. Svensson, E.C., et al. 2000. A syndrome of tricuspid atresia in mice with a targeted mutation of the gene encoding Fog-2. *Nat. Genet.* **25**:353–356.
11. Tevosian, S.G., et al. 2000. FOG-2, a cofactor for GATA transcription factors, is essential for heart morphogenesis and development of coronary vessels from epicardium. *Cell.* **101**:729–739.
12. Cantor, A.B., and Orkin, S.H. 2005. Coregulation of GATA factors by the Friend of GATA (FOG) family of multitype zinc finger proteins. *Semin. Cell Dev. Biol.* **16**:117–128.
13. Crispino, J.D., et al. 2001. Proper coronary vascular development and heart morphogenesis depend on interaction of GATA-4 with FOG cofactors. *Genes Dev.* **15**:839–844.
14. Manuylov, N.L., Smagulova, F.O., and Tevosian, S.G. 2007. Fog2 excision in mice leads to premature mammary gland involution and reduced Esr1 gene expression. *Oncogene.* **26**:5204–5213.
15. Moses, K.A., DeMayo, F., Braun, R.M., Reecy, J.L., and Schwartz, R.J. 2001. Embryonic expression of an Nkx2-5/Cre gene using ROSA26 reporter mice. *Genesis.* **31**:176–180.
16. Gaussin, V., et al. 2002. Endocardial cushion and myocardial defects after cardiac myocyte-specific conditional deletion of the bone morphogenetic protein receptor ALK3. *Proc. Natl. Acad. Sci. U. S. A.* **99**:2878–2883.
17. Epstein, J.A., and Parmacek, M.S. 2005. Recent advances in cardiac development with therapeutic implications for adult cardiovascular disease. *Circulation.* **112**:592–597.
18. Srivastava, D. 2006. Making or breaking the heart: from lineage determination to morphogenesis. *Cell.* **126**:1037–1048.
19. Zhou, B., et al. 2008. Epicardial progenitors contribute to the cardiomyocyte lineage in the developing heart. *Nature.* **454**:109–113.
20. Winter, E.M., and Gittenberger-de Groot, A.C. 2007. Epicardium-derived cells in cardiogenesis and cardiac regeneration. *Cell. Mol. Life Sci.* **64**:692–703.
21. Katz, S.G., et al. 2003. Endothelial lineage-mediated loss of the GATA cofactor Friend of GATA 1 impairs cardiac development. *Proc. Natl. Acad. Sci. U. S. A.* **100**:14030–14035.
22. Danielian, P.S., Muccino, D., Rowitch, D.H., Michael, S.K., and McMahon, A.P. 1998. Modification of gene activity in mouse embryos in utero by a tamoxifen-inducible form of Cre recombinase. *Curr. Biol.* **8**:1323–1326.
23. Gittenberger-de Groot, A.C., Vrancken Peeters, M.P., Mentink, M.M., Gourdie, R.G., and Poelmann, R.E. 1998. Epicardium-derived cells contribute a novel population to the myocardial wall and the atrioventricular cushions. *Circ Res.* **82**:1043–1052.
24. Wilm, B., Ipenberg, A., Hastie, N.D., Burch, J.B., and Bader, D.M. 2005. The serosal mesothelium is a major source of smooth muscle cells of the gut vasculature. *Development.* **132**:5317–5328.
25. Rouf, R., et al. 2008. Increased FOG-2 in failing myocardium disrupts thyroid hormone-dependent SERCA2 gene transcription. *Circ. Res.* **103**:493–501.
26. Wencker, D., et al. 2003. A mechanistic role for cardiac myocyte apoptosis in heart failure. *J. Clin. Invest.* **111**:1497–1504.
27. Yamamoto, S., et al. 2003. Activation of Mst1 causes dilated cardiomyopathy by stimulating apoptosis without compensatory ventricular myocyte hypertrophy. *J. Clin. Invest.* **111**:1463–1474.
28. Shiojima, I., et al. 2005. Disruption of coordinated cardiac hypertrophy and angiogenesis contributes to the transition to heart failure. *J. Clin. Invest.* **115**:2108–2118.
29. Lavine, K.J., and Ornitz, D.M. 2008. Fibroblast growth factors and Hedgehogs: at the heart of the epicardial signaling center. *Trends Genet.* **24**:33–40.
30. Lavine, K.J., et al. 2005. Endocardial and epicardial derived FGF signals regulate myocardial proliferation and differentiation in vivo. *Dev. Cell.* **8**:85–95.
31. Wu, H., Lee, S.H., Gao, J., Liu, X., and Iruela-Arispe, M.L. 1999. Inactivation of erythropoietin leads to defects in cardiac morphogenesis. *Development.* **126**:3597–3605.
32. Merki, E., et al. 2005. Epicardial retinoid X receptor alpha is required for myocardial growth and coronary artery formation. *Proc. Natl. Acad. Sci. U. S. A.* **102**:18455–18460.
33. Hirota, H., et al. 1999. Loss of a gp130 cardiac muscle cell survival pathway is a critical event in the onset of heart failure during biomechanical stress. *Cell.* **97**:189–198.
34. Hannenhalli, S., et al. 2006. Transcriptional genomics associates FOX transcription factors with human heart failure. *Circulation.* **114**:1269–1276.
35. Mustapha, Z., Pang, L., and Nattel, S. 2007. Characterization of the cardiac KCNE1 gene promoter. *Cardiovasc. Res.* **73**:82–91.
36. Cai, C.L., et al. 2008. A myocardial lineage derives from Tbx18 epicardial cells. *Nature.* **454**:104–108.
37. Carmeliet, P. 2005. Angiogenesis in life, disease and medicine. *Nature.* **438**:932–936.
38. Murakami, M., et al. 2008. The FGF system has a key role in regulating vascular integrity. *J. Clin. Invest.* **118**:3355–3366.
39. Li, D., et al. 2009. VEGF regulates FGF-2 and TGF-beta1 expression in injury endothelial cells and mediates smooth muscle cells proliferation and migration. *Microvasc. Res.* **77**:134–142.
40. Malabanan, K.P., Kanellakis, P., Bobik, A., and Khachigian, L.M. 2008. Activation transcription factor-4 induced by fibroblast growth factor-2 regulates vascular endothelial growth factor-A transcription in vascular smooth muscle cells and mediates intimal thickening in rat arteries following balloon injury. *Circ. Res.* **103**:378–387.
41. Holmes, D.I., and Zachary, I.C. 2008. Vascular endothelial growth factor regulates stanniocalcin-1 expression via neuropilin-1-dependent regulation of KDR and synergism with fibroblast growth factor-2. *Cell Signal.* **20**:569–579.
42. Folkman, J. 2006. Antiangiogenesis in cancer therapy--endostatin and its mechanisms of action. *Exp. Cell Res.* **312**:594–607.
43. Mundel, T.M., and Kalluri, R. 2007. Type IV collagen-derived angiogenesis inhibitors. *Microvasc. Res.* **74**:85–89.
44. Eklund, L., et al. 2001. Lack of type XV collagen causes a skeletal myopathy and cardiovascular defects in mice. *Proc. Natl. Acad. Sci. U. S. A.* **98**:1194–1199.
45. Zhou, B., et al. 2006. G-CSF-mobilized peripheral blood mononuclear cells from diabetic patients augment neovascularization in ischemic limbs but with impaired capability. *J. Thromb. Haemost.* **4**:993–1002.
46. Ma, Q., Zhou, B., and Pu, W.T. 2008. Reassessment of Isl1 and Nkx2-5 cardiac fate maps using a Gata4-based reporter of Cre activity. *Dev. Biol.* **323**:98–104.
47. Mitchell, G.F., Jeron, A., and Koren, G. 1998. Measurement of heart rate and Q-T interval in the conscious mouse. *Am. J. Physiol.* **274**:H747–H751.